Lower plate structure and upper plate deformational segmentation at the Sunda-Banda arc transition, Indonesia

L. Planert,[1] H. Kopp,[1] E. Lueschen,[2] C. Mueller,[2] E. R. Flueh,[1] A. Shulgin,[1] Y. Djajadihardja,[3] and A. Krabbenhoeft[1]

Received 22 June 2009; revised 23 April 2010; accepted 29 April 2010; published 27 August 2010.

[1] The Sunda-Banda arc transition at the eastern termination of the Sunda margin (Indonesia) represents a unique natural laboratory to study the effects of lower plate variability on upper plate deformational segmentation. Neighboring margin segments display a high degree of structural diversity of the incoming plate (transition from an oceanic to a continental lower plate, presence/absence of an oceanic plateau, variability of subducting seafloor morphology) as well as a wide range of corresponding fore-arc structures, including a large sedimentary basin and an accretionary prism/outer arc high of variable size and shape. Here, we present results of a combined analysis of seismic wide-angle refraction, multichannel streamer and gravity data recorded in two trench normal corridors located offshore the islands of Lombok (116°E) and Sumba (119°E). On the incoming plate, the results reveal a 8.6–9.0 km thick oceanic crust, which is progressively faulted and altered when approaching the trench, where upper mantle velocities are reduced to ~7.5 km/s. The outer arc high, located between the trench and the fore-arc basin, is characterized by sedimentary-type velocities (Vp < 5.5 km/s) down to the top of the subducting slab (~13 km depth). The oceanic slab can be traced over 70–100 km distance beneath the fore arc. A shallow serpentinized mantle wedge at ~16 km depth offshore Lombok is absent offshore Sumba, where our models reveal the transition to the collisional regime farther to the east and to the Sumba block in the north. Our results allow a detailed view into the complex structure of both the deeper and shallower portions of the eastern Sunda margin.

Citation: Planert, L., H. Kopp, E. Lueschen, C. Mueller, E. R. Flueh, A. Shulgin, Y. Djajadihardja, and A. Krabbenhoeft (2010), Lower plate structure and upper plate deformational segmentation at the Sunda-Banda arc transition, Indonesia, *J. Geophys. Res.*, *115*, B08107, doi:10.1029/2009JB006713.

1. Introduction

[2] The Sunda-Banda arc transition comprises the portions of the Indonesian island arc where the tectonic regime changes from oceanic-island arc subduction along the eastern Sunda arc to continent-island arc collision along the Banda arc (Figure 1). Such a setting offers a broad spectrum of tectonic/geologic variation regarding the lower plate as well as the upper plate, which makes this plate boundary an ideal target to study detailed aspects of subduction zone processes.

[3] Scientific investigations at subduction zones conducted during recent years have increasingly put their focus on the physical interaction between the lower plate and the fore arc and related aspects of material transfer and balancing. The physical and chemical properties of the lower plate, including its crustal and mantle structure/composition, fluid content, sedimentary cover, and thermal character (plate age), as well as the convergence rate are essential to processes of accretion, erosion and arc magmatism of the upper plate (see *Clift and Vannucchi* [2004] for a review). However, modern seismic and acoustic data are still rare for the eastern Sunda arc and the transition to the Banda arc and hence, this study aims at providing a clearer picture of the area's tectonic setting.

[4] Subduction zones may grow by frontal or basal accretion and may be classified as a compressive regime. Extension and large-scale subsidence on the contrary originate from erosive processes, which are often favored by a rough seafloor topography and a sediment-starved deep sea trench. Thus a change from an accretionary to a non-accretionary/erosive regime may be expected, concurrent with a change in the tectonic evolution of fore-arc structure. The eastern Sunda arc comprises a well-developed outer arc high and a major fore-arc basin (Lombok Basin). The deeper

[1]IFM-GEOMAR, Leibniz Institute of Marine Sciences at the University of Kiel, Kiel, Germany.
[2]BGR, Federal Institute for Geosciences and Natural Resources, Hannover, Germany.
[3]BPPT, Agency for the Assessment and Application of Technology, Jakarta, Indonesia.

0148-0227/10/2009JB006713

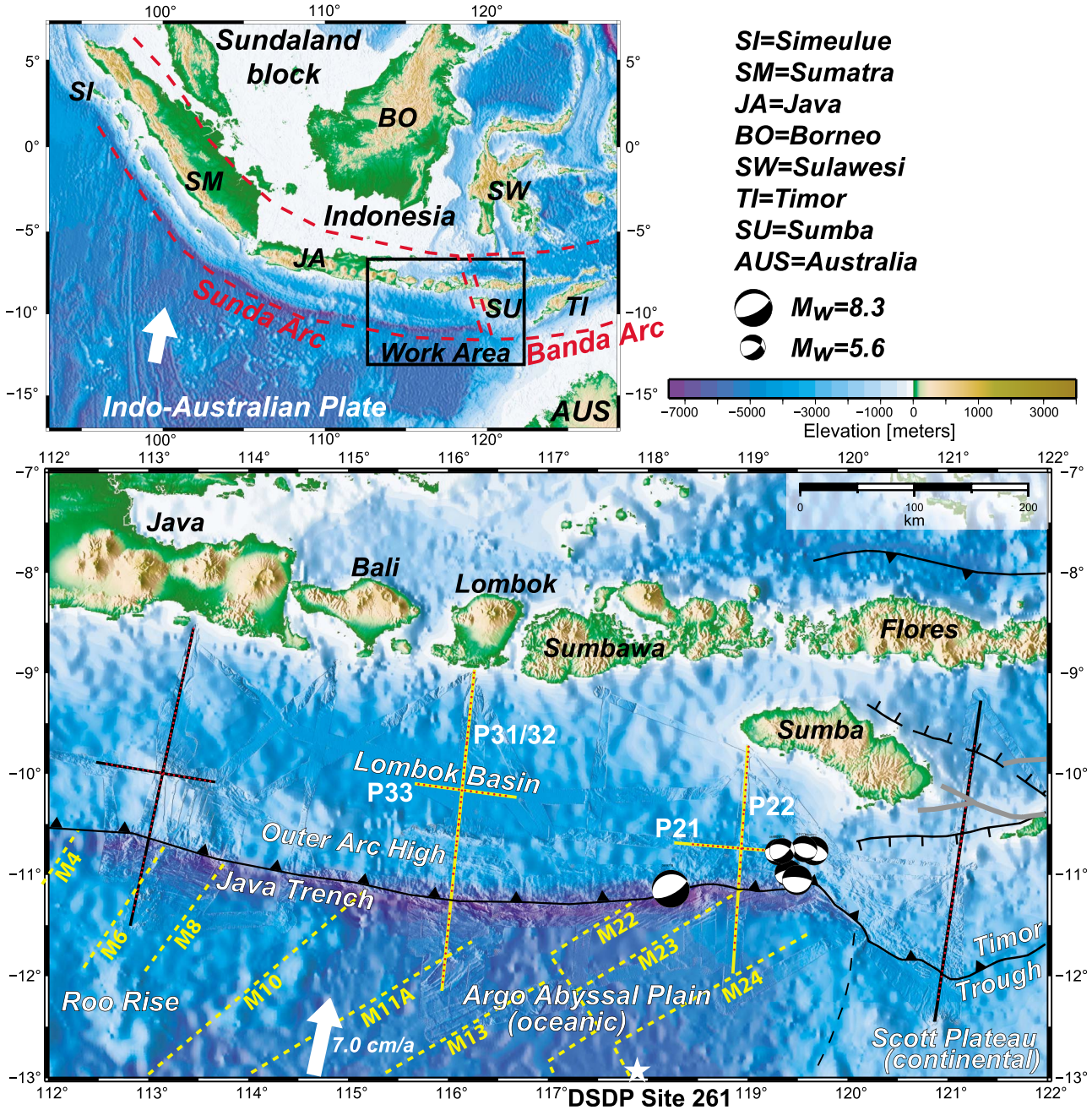

Figure 1. Regional map with features discussed in the text and close-up of work area with profile distribution of the SINDBAD seismic refraction experiment. Red points mark the locations of ocean bottom seismic recorders. In this study we present results for the corridors at 116°E and 119°E (yellow profiles) characterized by the subduction of oceanic crust of the Argo Abyssal Plain. The westernmost (113°E) as well as easternmost (121°E) corridors (black profiles) represent distinct tectonic regimes dominated by the subduction of thickened crust of the Roo Rise and Scott Plateau, respectively. The 121°E corridor is discussed in the work of *Shulgin et al.* [2009] and Shulgin et al (submitted manuscript, 2010). Focal mechanisms correspond to Mw = 8.3 main shock and 4 days aftershock series of the 1977 Sumba earthquake (http://www.globalcmt.org). Yellow dashed lines display magnetic anomalies from *Müller et al.* [2008]. Plate convergence is (white arrow) from *Simons et al.* [2007].

structure of these features is, however, not yet resolved and their origin is still not fully understood.

[5] Near the trench, the formation and reactivation of faults is related to the bending of the oceanic plate and often results in the hydratization of the oceanic crust and mantle [e.g., *Ranero et al.*, 2003]. The 1977 Sumba earthquake, one of the largest normal-faulting earthquakes (Mw = 8.3) near an oceanic trench, occurred at the extreme eastern limb of the Java trench in our study area (Figure 1). Hence, it provides an opportunity to examine the amount and depth

extent of lower plate alteration as response to large bending stresses. Possible dewatering processes in the lower plate during subduction may also control the long-term tectonics of the fore arc, because these processes are pertinent to the functioning of seismogenic zones [e.g., *Peacock*, 2001; *Bostock et al.*, 2002; *Ranero et al.*, 2008]. At the eastern Sunda arc, there is a historical absence of large interface thrust earthquakes in a strip of 50–150 km between the along-trench seismicity and the onset of the Wadati-Benioff zone, which still requires further explanation [e.g., *Špičák et al.*, 2007].

[6] The seismic and acoustic measurements, combined with gravimetric studies, conducted during R/V *Sonne* cruise SO190 allow a quantification of the "raw materials" (seafloor sediments, oceanic crust and mantle lithosphere), which are carried into the system at the deep sea trench, but also investigate the complex structure of the adjacent fore arc up to close to the volcanic arc. The results of this study may offer insights into the role of the lower plate, as the point of origin in the "subduction factory", as well as into the reactions and consequences for the tectonic evolution of the overriding plate.

2. Tectonic Setting

[7] Convergence between the Indo-Australian Plate in the south and the Eurasian Plate in the north is active since the late Oligocene [*Hamilton*, 1988; *Hall and Smyth*, 2008] and currently occurs at a rate of ~70 mm/yr in N13°E direction offshore Bali [*Simons et al.*, 2007]. Eastward from about 121°E, however, the relative motion at the Timor Trough has slowed down to ~15 mm/yr, and the development of back-arc thrusts appears to account for sustained northward motion of Australian lithosphere [*Bock et al.*, 2003] (Figure 1). The seismic profile offshore Flores from *Shulgin et al.* [2009] shows a 12–15 km thick crust comprising the promontory of the Australian continental shelf, which currently underthrusts beneath the Banda fore arc, resulting into thickening and uplift of the outer arc ridge. Hence, conventional subduction cannot be occurring here.

[8] The transition from the Scott Plateau, which is marked by shallower seafloor depths and increased sedimentary coverage on the Australian continental shelf, to the oceanic lithosphere comprising the Argo Abyssal Plain occurs at ~120°E (Figure 1). The 1977 Sunda earthquake series [e.g., *Spence*, 1986] occurred at this transition region in the oceanic plate. Relocation of hypocenters and focal mechanisms are consistent with normal faulting throughout the upper 28 km of oceanic lithosphere (Figure 1). The earthquake produced a 10 m tsunami wave height on the island of Sumbawa, which suggests substantial deformation of the ocean bottom and associated fault displacement at very shallow depths. The aftershock area implies at least 200 km of fault rupture, with a concentration of aftershocks ~100 km northeast of the main shock close to the termination of the Java trench, where the underthrust Scott Plateau could have acted as a rupture barrier [*Spence*, 1986; *Lynnes and Lay*, 1988]. *Spence* [1986] attributes the origin of the large tensional stresses which caused the Sumba earthquake series to large bending stresses of slab-pull origin, facilitated by increased resistance to subduction of the adjacent Scott Plateau. Yet the resulting consequences of the inferred large bending stresses on the structure of the subducting oceanic lithosphere in this area are unresolved.

[9] Seafloor age of the oceanic lithosphere increases toward the east from Early Cretaceous at 110°E to Late Jurassic close to 120°E [*Heine et al.*, 2004; *Müller et al.*, 2008]. The trend of magnetic seafloor anomalies is ~45–60° and thus oblique to the relative plate motion, which is almost perpendicular to the trench (Figure 1). The westernmost portions of our study area comprise the branches of an oceanic plateau, the Roo Rise, which is characterized by seafloor up to 1500 m shallower compared to the adjacent seafloor of the Argo Abyssal Plain.

[10] Fore-arc structures along this margin include a well-developed outer arc high (OAH) which is visible as a continuous bathymetric feature along the entire Indonesian fore arc, starting with Simeulue island offshore northern Sumatra as its subaerial expression and continuing as a submarine bathymetric elevation from offshore western Java to offshore the island of Sumba (Figure 1). The observed decrease in dimension and height of the OAH toward the east is related to the younger age of the eastern Sunda margin [e.g., *Van der Werff*, 1995] and to changes in trench sediment contribution and subducting seafloor morphology of the incoming Indo-Australian Plate. The related subduction processes at the plate boundary result in an accretionary regime offshore Sumatra and western Java [*Schlüter et al.*, 2002; *Kopp and Kukowski*, 2003], whereas erosive processes dominate off central and eastern Java, where the subduction of the Roo Rise results in a northward retreat of the trench and the OAH [*Kopp et al.*, 2006]. Farther east offshore Lombok and Sumbawa, however, the sediment input to the trench as well as the internal structure of the oceanic crust are largely unknown and as a consequence the processes governing the origin and evolution of the OAH are still unclear. A good indication of sediment origin and thickness farther south in the Argo Abyssal Plain can be gained from the results of DSDP site 261 (Figure 1), which drilled into a rugged oceanic basement of late Jurassic age at ~530 m below seafloor covered by Cretaceous claystones, Upper Miocene and Pliocene nannofossil oozes and Quaternary radiolarian clays [*Heirtzler et al.*, 1974].

[11] The overriding plate is of continental nature off Sumatra [*Kopp et al.*, 2001] and changes to an island arc type off Java/Lombok and farther east, although the internal structure of the islands and the adjacent fore arc is still largely unknown due to the lack of deep seismic data. The Lombok Basin forms a major fore-arc basin and is located between the OAH and the volcanic arc in the north (Figure 1). Its termination in the west is controlled by the subduction of the Roo Rise and related uplift of the adjacent fore arc [*Kopp et al.*, 2006] and in the east by the collision of the Australian continental shelf with the crystalline basement comprising the island of Sumba [*Shulgin et al.*, 2009]. The origin of Sumba is still enigmatic; it is not part of the modern Banda volcanic arc but according to a number of investigators [e.g., *Rutherford et al.*, 2001; *Hall*, 2002] originated at a relict northern hemispheric arc system, situated south of West Sulawesi. The island migrated to its current position in the middle to late Miocene, as response to incipient collision with Australia, and now forms an integral part of the fore arc.

[12] In 2006, R/V *Sonne* cruise SO190 investigated the Sunda-Banda arc transition during two consecutive legs within the scope of the Seismic and Geoacoustic Investigations Along the Sunda-Banda Arc Transition (SINDBAD) project. During leg 1, almost 5000 km of multichannel streamer (MCS) seismic data and coincident shipboard gravity data were acquired between 112°E and 122°E. The MCS data are discussed in the work of *Lüschen et al.* [2010]. Leg 2 included the acquisition of more than 1700 km of wide-angle reflection and refraction seismic profiles in four different corridors of the margin (Figure 1), at 113°E (offshore eastern Java), 116°E (offshore Lombok), 119°E (offshore Sumba) and 121°E (offshore Flores). Additionally, seafloor swath mapping on both legs resulted in an almost complete coverage of the trench and the lower slope between 113°E and 121°E. The westernmost (113°E) as well as easternmost (121°E) corridors represent distinct tectonic regimes dominated by the subduction of thickened crust of the Roo Rise and Scott Plateau, respectively. The 121°E area is discussed in the work of *Shulgin et al.* [2009] and A. Shulgin et al. (Structural architecture of oceanic plateau subduction offshore Eastern Java and the potential implications for geohazards, submitted to *Geophysical Journal International*, 2010). In this study we present results from the analysis of deep penetrating seismic and shipboard gravity data to resolve the internal structure of the incoming and the overriding plates for the corridors at 116°E and 119°E.

3. Bathymetric Features

[13] At 116°E offshore Lombok, seafloor depths on the incoming oceanic plate are in the range of 5.0–5.5 km and reach up to 6.8 km in the trench. In the Argo Abyssal Plain, basement structures can be traced on the seafloor, aligned at angles of 45–60° and subparallel to the magnetic anomalies (Figure 1). Hence, these structures most likely correspond to original seafloor fabric imprinted during seafloor spreading. For distances less than ~40 km seaward of the trench, however, the prevailing strike of basement structures changes to a more trench parallel tectonic fabric (compare white-dashed lines in Figure 2), which may reflect recent activity and the onset of plate-bending related normal faulting in the oceanic plate.

[14] Where our seismic profile crosses the trench, the deformation front reveals a local indentation, indicating the erosion of the lowermost inner trench slope. Farther east, however, equivalent portions of the inner trench wall (>5 km depths) appear to be rather undisturbed. Here, more than three arrays of trench-parallel ridges and troughs suggest the presence of a frontal imbricate fan (Figure 2).

[15] Landward of the trench, the OAH seafloor rises up to water depths of 2.4 km (slope angle ~5°). Corresponding seafloor portions are characterized by a trench-parallel tectonic fabric including two pronounced ridges spaced ~25 km apart (Figure 2). On a MCS seismic profile located at ~114°E, *Müller et al.* [2008] identified recent vertical displacements of the seafloor and associated deformation at shallow depths as manifested in the uplift and tilting of small piggyback basins between the two tectonic ridges atop of the OAH. These structures are associated with landward dipping splay faults, which penetrate the entire crust and connect to the plate interface. The importance of such faults for tsunami generation during great subduction zone earthquakes was recently demonstrated for Sumatra [*Sibuet et al.*, 2007], North Ecuador [*Collot et al.*, 2008] and Nankai [*Moore et al.*, 2007]. North of the OAH, the Lombok Basin exhibits a very smooth and virtually flat seafloor with water depths of 4.4 km.

[16] At 119°E offshore Sumba, water depths are slightly shallower for the oceanic plate and the trench (4.8–5.0 km and 6.5 km) and the corresponding seafloor is smoothed by a sediment blanket for distances >30 km seaward of the trench (Figure 2). Farther north, seafloor morphology changes abruptly, where a series of northward dipping normal faults induces intense fracturing and stepwise downflexure of the oceanic crust at the outer trench wall. In the trench, however, two faults, dipping to the south and striking at low angles relative to the trench, subduct beneath the inner trench wall, which results in pronounced indentations of the deformation front and the adjacent slope (Figure 2). The strike of these features is ~65°, i.e., subparallel to the magnetic anomalies. The 1977 Sumba earthquake epicenter [*Engdahl and Villaseñor*, 2002] is located roughly where the western fault subducts beneath the inner trench wall. The focal mechanism of the main shock (strike angle 61°; dip angle 67°; slip angle −98°; Global CMT Catalog, http://www.globalcmt.org) and the location of aftershocks with respect to the main shock (Figure 1) are consistent with a rupture zone striking at low angles relative to the trench. Hence, theses data suggest a possible link between plate-bending related normal faulting, extending to perhaps 30–50 km depth [*Spence*, 1986; *Lynnes and Lay*, 1988], and the reactivation of inherited fault structures in the oceanic crust, as indicated by the observed trend oblique to the trench and subparallel to the magnetic anomalies. Fan-shaped slide deposits with a lateral dimension of ~25 km are visible ~30 km east of where our profile crosses the trench (Figure 2). We speculate that this slide was caused by slope failure due to the subduction of equivalent seafloor fabric.

[17] Offshore Sumba, the lateral and vertical dimensions of the outer arc high are smaller (~55 km compared to ~80 km offshore Lombok) and the transition in seafloor topography from the elevated segments toward the adjacent fore-arc portions in the north is much more subdued (Figure 2).

4. Seismic Data

[18] Offshore Lombok, profile 31/32 consists of two overlapping profiles and runs perpendicular to the trench reaching a full length of 354 km (Figure 2). A total of 46 IFM-GEOMAR ocean bottom hydrophones/seismometers (OBH/S) [*Bialas and Flueh*, 1999] were deployed on this line at ~6 km average instrument spacing. The profile extends from 100 km seaward of the trench to close to the island of Lombok, crossing the Lombok Basin and profile 33 at ~222 km profile distance. Profile 33 runs in a trench-parallel direction and covers a 113 km long portion of the Lombok Basin. On this line, 16 OBH/S were deployed at ~6 km instrument spacing.

[19] The 119°E corridor offshore Sumba comprises two additional seismic profiles: the 250 km long trench-perpendicular profile 22 and the 145 km long crossing profile 21, covered with 27 and 18 OBH/S at ~6 km

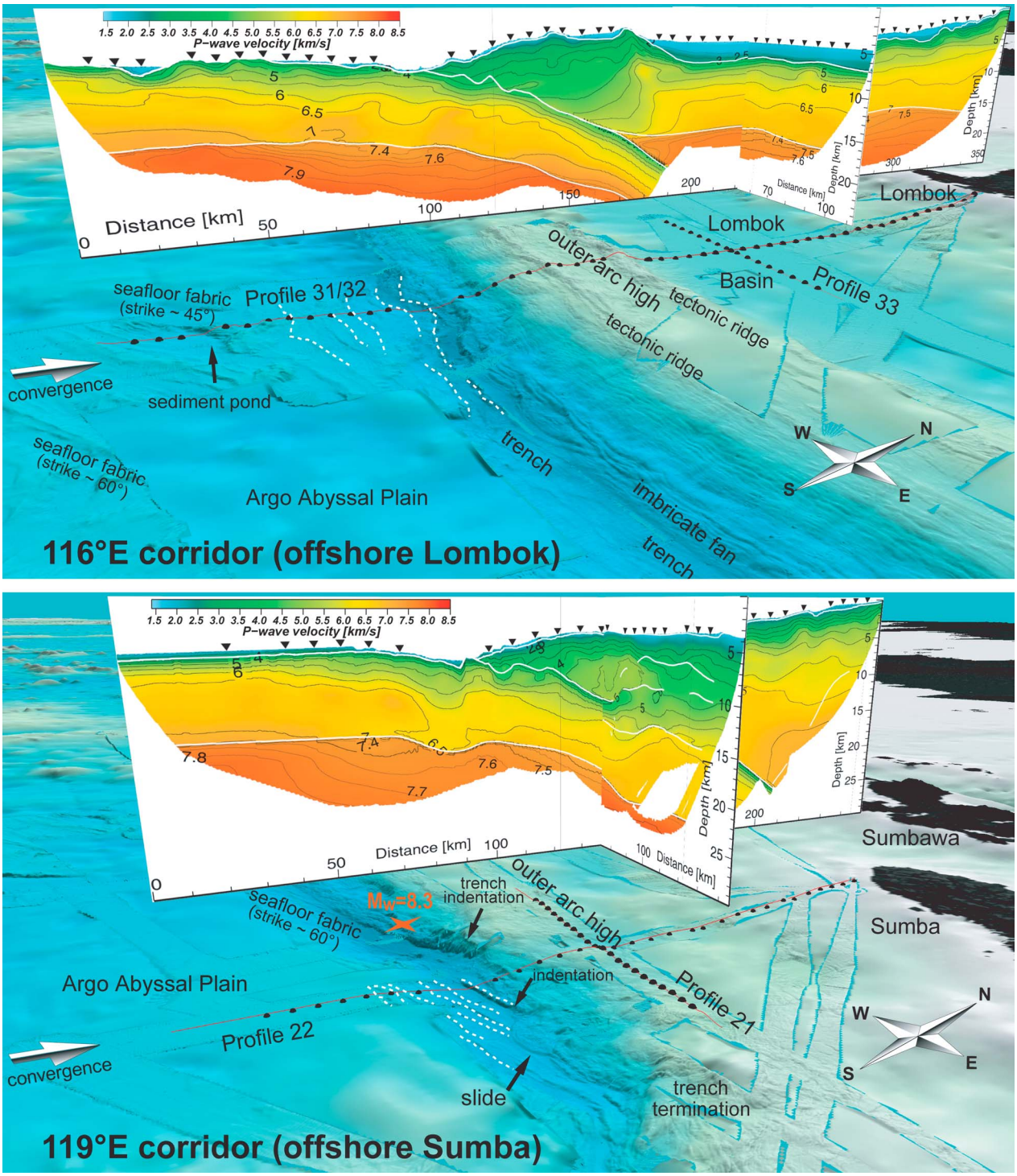

Figure 2. Perspective views of the (top) 116°E and (bottom) 119°E corridors including acquired seafloor bathymetry and seismic velocity profiles. The red lines are seafloor projections of the seismic shots; black spheres mark the instrument locations. Seafloor fabric locally crops out as basement structures on the oceanic plate. Offshore Lombok, inherited seafloor fabric strikes at angles of 45°–60°; plate-bending related normal faults trend more parallel to the trench (white dashed lines). The trench is largely devoid of sediment. A well-developed outer arc high comprises pronounced ridge structures. The Lombok Basin is characterized by a virtually flat seafloor. Offshore Sumba, inherited seafloor fabric strikes at angles of 60°–70° and seems to be reactivated as response to plate bending (red star marks epicenter of 1977 Sumba main shock). The subduction of basement structures locally results in the erosion of the lower slope and subsequent slope failure (note the coincidence of the eastern indentation and the slide). Annotated features are discussed in the text.

instrument spacing, respectively (Figure 2). Line 21 covers the OAH at its highest elevation.

[20] The seismic source used for wide-angle profiling was an eight element 64 l G-gun cluster fired at 3000 psi in constant time intervals, resulting in a nominal shot spacing of 130 m. Data processing included the localization of the ocean bottom instruments using the arrival time of the direct wave and the exact shot point geometry. In a second step, a time-gated deconvolution was applied to remove predictable bubble reverberations to produce a signal free of the disturbing interference of multiple and primary phases [*Wiener*, 1949]. Finally, a time and offset-variant Butterworth filter was applied in which the passband moves toward lower frequencies as record time and offset increases to account for frequency changes caused by signal attenuation.

[21] For the seismic velocity analysis we chose the tomographic method of *Korenaga et al.* [2000] (TOMO2D), which determines the 2-D velocity structure together with a floating reflector from the simultaneous inversion of refracted and reflected phases. The method employs a hybrid ray-tracing scheme combining the graph method with further refinements utilizing ray bending with the conjugate gradients method. Smoothing and damping constraints regularize the iterative inversion. The velocity model is defined as an irregular grid hung from below the seafloor. We used a horizontal node spacing of 250 m and a vertical node spacing, which linearly increases from 100 m at the seafloor to 250 m at 30 km depth below seafloor. Model regularization is accomplished by the use of correlation lengths, which control the size of those model areas affected by a velocity update of a grid cell [*Korenaga et al.*, 2000]. We used a horizontal correlation length, which linearly increases from 1.5 km at the seafloor to 6 km at the model bottom, and a vertical correlation length with corresponding values of 0.2 km and 1.5 km, respectively. For reflector nodes, the appropriate regularization length scales are taken from the horizontal 2-D velocity correlation lengths at the corresponding depths.

[22] From the coincident MCS seismic profiles we incorporated the well resolved sedimentary portions as a priori structure into our starting models and fixed these areas during the iterations using spatially variable velocity damping. To make use of secondary arrivals and different reflections we utilized a "layer stripping" approach and subsequently built the velocity model from top to bottom. This approach further involves the use of spatially variable velocity damping for the upper layers, e.g., when restricting the picks to the lower layers, and the incorporation of velocity jumps into the input models at primary features such as the basement, plate boundary and the crust-mantle boundary (Moho). In practice, we used a 1-D velocity starting model and inverted first for the upper units (fore arc, outer arc high) down to the next major structural interface (fore-arc Moho, plate boundary). We then again used a 1-D velocity starting model for the inversion of the next deeper unit (fore-arc mantle, oceanic crust, oceanic mantle). RMS travel time misfits for the final velocity models shown here are in the range of 60 ms for a total of 9.000 (profile 21) to 26.000 (profile 31/32) arrivals, which were manually picked and assigned with individual pick uncertainties in the processed seismic sections (see Figures 3 and 4 for data examples of profile 31/32).

4.1. Profile 31/32

[23] Figure 5 shows the final tomographic solution of profile 31/32, the corresponding derivative weight sum (DWS), which is a measure of ray density in the neighborhood of a model node [*Toomey and Foulger*, 1989], and the coincident prestack depth-migrated (PSDM) MCS profile from *Lüschen et al.* [2010]. The incoming oceanic crust is on average 8.6 km thick and largely devoid of sediment, except for an isolated sediment pond at ~20 km profile distance (Figure 5a). This sediment accumulation occurs in a structural trap related to the original seafloor fabric imprinted during seafloor spreading (compare Figure 2). About 40–50 km seaward of the trench velocities start to decrease in the crust and in the underlying mantle, resulting in anomalously low mantle velocities of ~7.5 km/s directly beneath the Moho (Figure 5a; see Figure 3 for data examples). The area of reduced velocities coincides with the onset of plate-bending related normal faulting in the MCS seismic data (Figure 5c; compare white-dashed lines in Figure 2).

[24] The OAH reveals relatively low velocities of 2.5–5.5 km/s above the plate boundary. The plate boundary is constrained by reflections in both the wide-angle and MCS seismic data over a distance of at least 70 km beneath the OAH down to ~15 km depth (dip: 5–8°) (Figure 6). The plate interface is of irregular shape, suggesting in places several hundreds of meters vertical displacement.

[25] The Lombok Basin is characterized by up to 2.8 km of sediment infill comprising velocities of 1.6–2.8 km/s (Figures 5 and 6). The underlying crust is 9–10 km thick and reveals a pronounced model portion with velocities of 6–6.8 km/s (see Figure 4 for data example). The transition from the low velocity portions beneath the OAH to velocities >5.5 km/s beneath the Lombok Basin occurs abruptly over a distance of 10–30 km around profile km 180 (Figure 6). Velocities in the upper fore-arc mantle are in the range of 7.4–7.8 km/s and thus significantly lower compared to those expected for unaltered mantle peridotite [*Carlson and Miller*, 2003].

[26] In order to demonstrate the resolving power of the data in different parts of the model, a synthetic test was performed where a known model has to be resolved using the same profile geometry and data coverage as in the real experiment. A set of Gaussian velocity anomalies of ±3% velocity perturbation and dimensions of 25 km × 5 km was imposed in a checkerboard pattern on the final velocity solution of profile 31/32 (Figure 7). Synthetic traveltimes were computed through this model and Gaussian noise with a standard deviation equal to a quarter of the individual pick uncertainty was added to the synthetic traveltimes. The inversion was initialized using the underlying velocity model as a starting model. The aim of this approach is to test the algorithm's capability of resolving small perturbations within the original tomographic output and whether anomalies are transferred into different areas during this process. Lower and upper plates were investigated separately, in order to incorporate reflections from the major interfaces and according to the tomographic approach chosen for these profiles. As displayed in the recovery panels of Figure 7, the incoming oceanic crust is well resolved, as is the oceanic uppermost mantle. Resolution of the upper plate

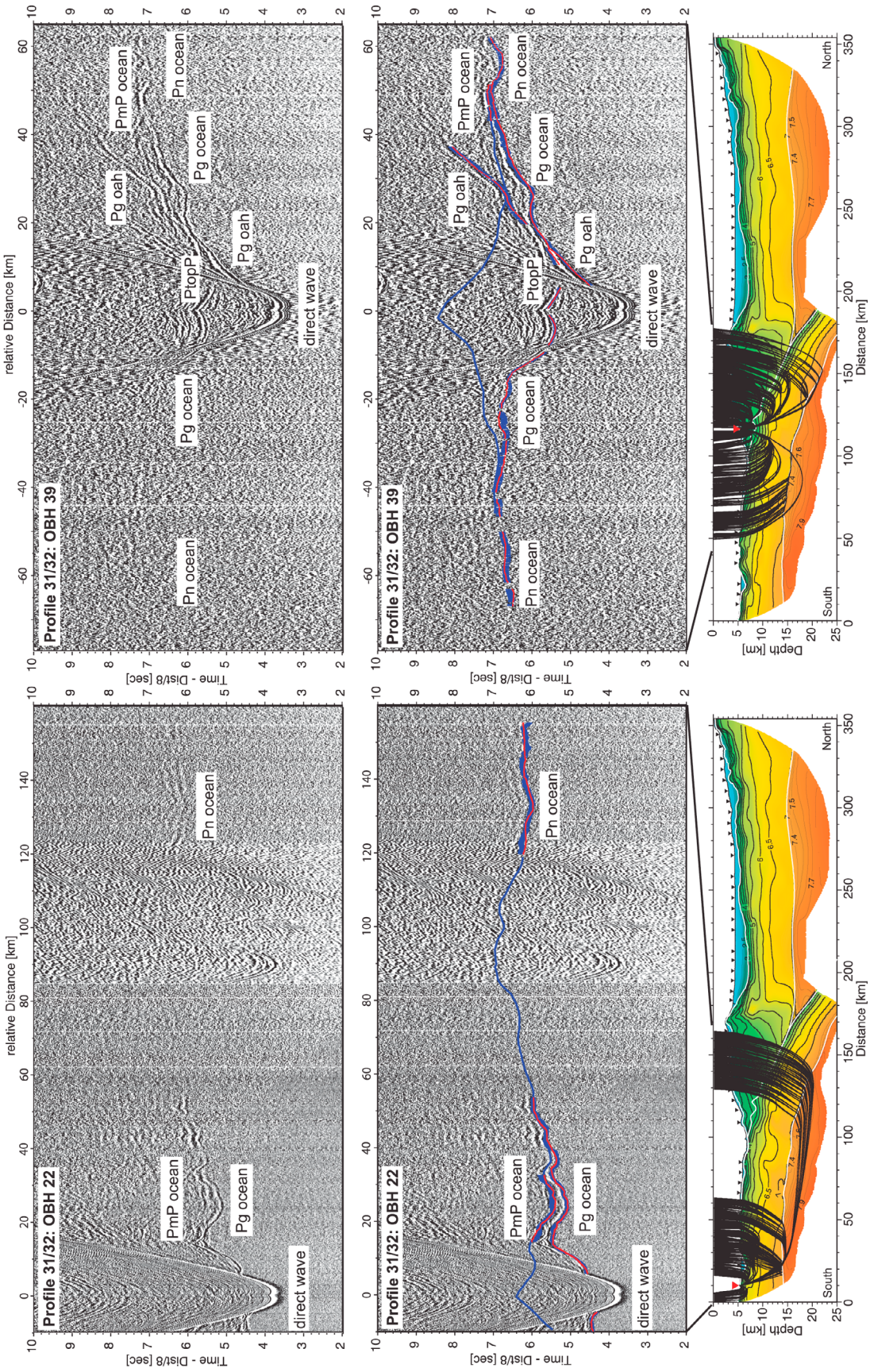

Figure 3. Seismic record sections (reduced to 8 km/s) of OBH 22 and OBH 39 on profile 31/32. (top) Interpreted seismic arrivals are labeled: Pg oah (turning rays within the outer arc high), Pg ocean (turning rays within the oceanic crust), Pn ocean (turning rays in the upper oceanic mantle), PtopP (reflected rays at the plate boundary), and PmP ocean (reflected rays at the oceanic Moho). (middle) Picks are shown as blue bars according to their pick uncertainty; computed traveltimes are shown as red dots. Blue lines represent traveltimes for offsets not constrained by picks. (bottom) Corresponding raypaths of the picked traveltimes through the final tomographic solution of profile 31/32.

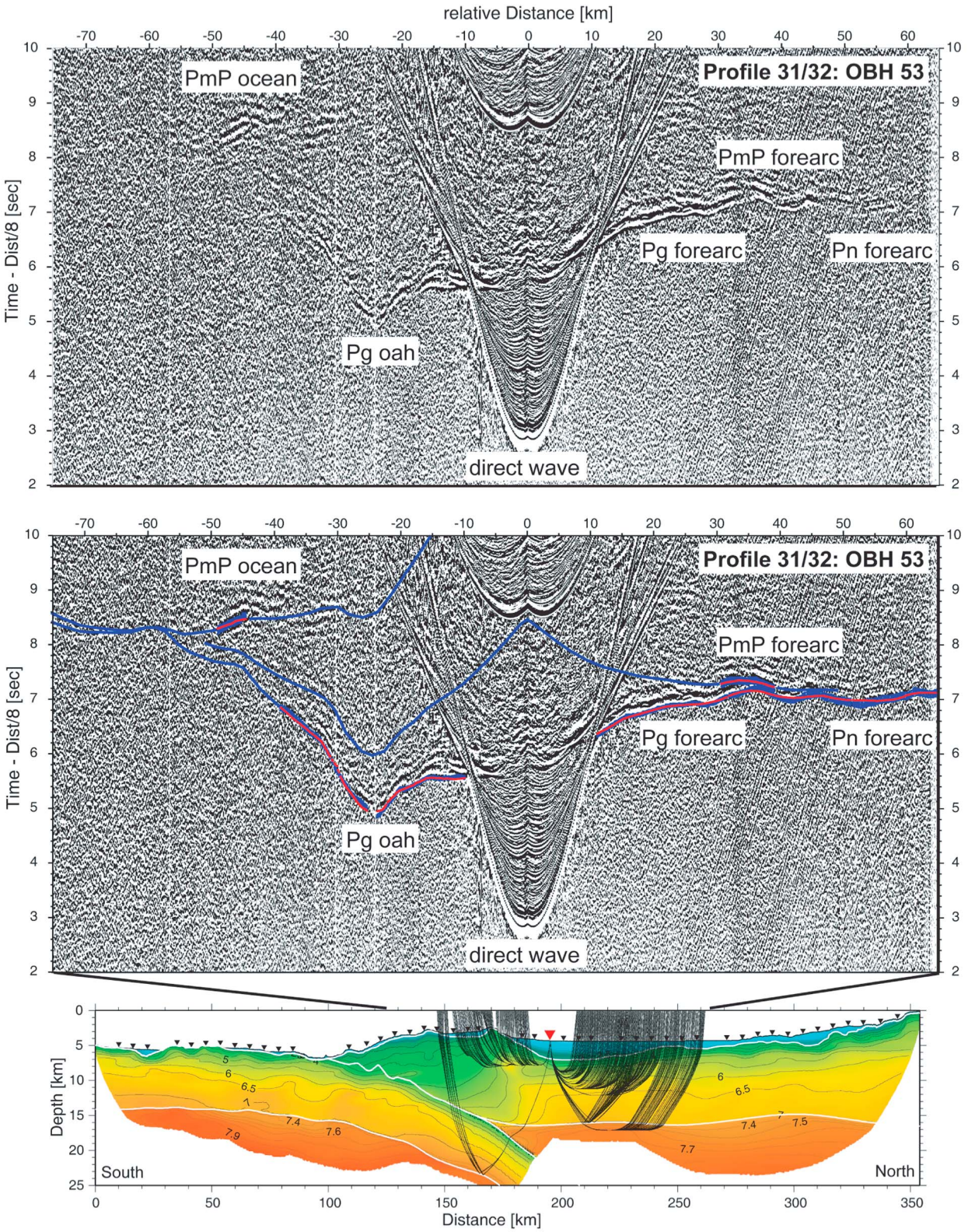

Figure 4. Seismic record section (reduced to 8 km/s) of OBH 53 on profile 31/32. (top) Interpreted seismic arrivals are labeled: Pg oah (turning rays within the outer arc high), Pg fore arc (turning rays within the fore-arc crust), Pn fore arc (turning rays in the upper fore-arc mantle), PmP fore arc (reflected rays at the fore-arc Moho), and PmP ocean (reflected rays at the oceanic Moho). (middle) Picks are shown as blue bars according to their pick uncertainty; computed traveltimes are shown as red dots. Blue lines represent traveltimes for offsets not constrained by picks. (bottom) Corresponding raypaths of the picked traveltimes through the final tomographic solution of profile 31/32.

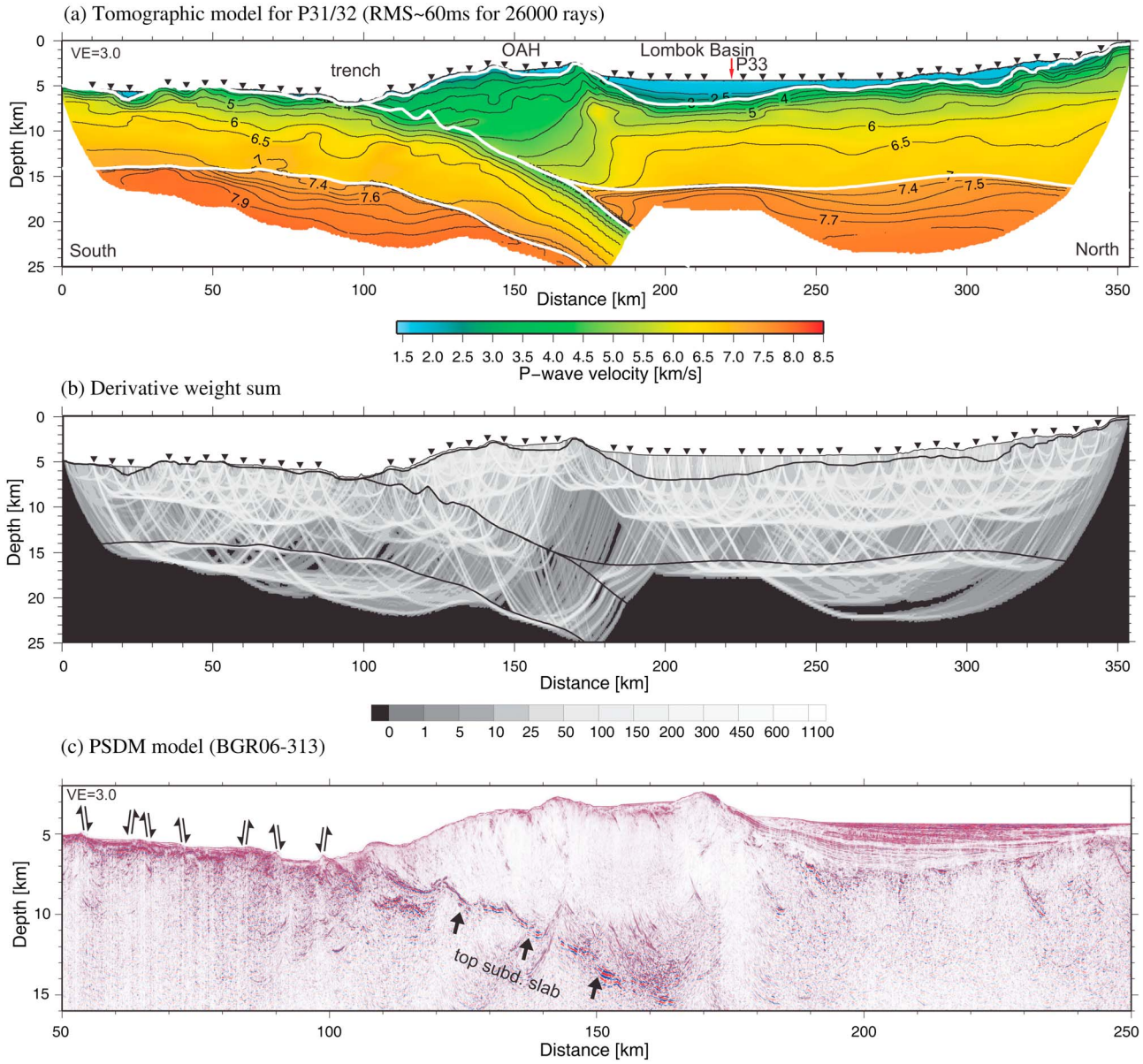

Figure 5. (a) Final tomographic velocity model of profile 31/32. Triangles indicate locations of ocean bottom seismographs. Red arrow displays line intersection with profile 33. White lines mark structural interfaces: sedimentary portions are derived from the analysis of high-resolution MCS seismic data; plate boundary, oceanic Moho and fore-arc Moho are obtained from the joint refraction and wide-angle reflection tomography. (b) Derivative weight sum for the final tomographic velocity model. (c) Prestack depth-migrated MCS line BGR06-313 from *Lüschen et al.* [2010]. All models are plotted at 3 × vertical exaggeration. OAH, outer arc high.

diminishes at a depth of 18 km, but the entire crust and upper mantle wedge are resolved (please refer to Figures S1 and S2 of the auxiliary material for additional resolution tests with synthetic anomalies confined to the oceanic mantle underneath the trench and an evaluation of the impact of different mantle starting models on the tomographic solution of profile 31/32).[1]

4.2. Profile 33

[27] On this line, the basement of the Lombok Basin is found in depths of 2.0 km to 3.7 km beneath the seafloor and resolved sediment velocities reach 2.8 km/s (Figure 8). Since no MCS seismic data are available for profile 33 also the sedimentary portions were modeled using refracted and wide-angle reflected seismic phases (see Figure 9 for data examples). The underlying crust shows some thickness variations around average values of 10 km and it includes a ~6 km thick portion of velocities of 6–6.8 km/s and relatively low velocity gradients. The velocities in the upper-

[1]Auxiliary materials are available in the HTML. doi:10.1029/2009JB006713.

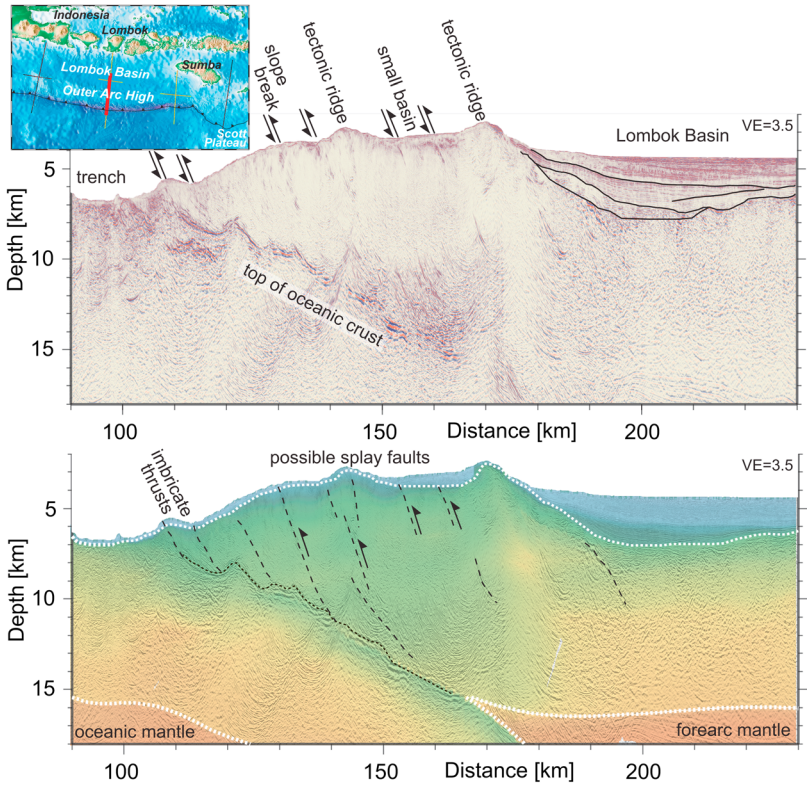

Figure 6. (top) Close-up of prestack depth-migrated MCS line BGR06-313 (modified from *Lüschen et al.* [2010]). The plate interface reveals a pronounced vertical relief. The outer arc high is characterized by landward dipping faults. (bottom) Final tomographic velocity model and line drawing overlain over PSDM image. Possible splay faults connect to the seafloor, where they are associated with changes in slope angle and tectonic ridges. Arrows indicate movement along faults. See text for discussion. Models are plotted at 3.5× vertical exaggeration.

most mantle are in the range of 7.4 km/s, reaching 7.7 km/s in 21 km depth and thus are slightly lower compared to profile 31/32 at the line intersection.

4.3. Profile 22

[28] In the southernmost model portions the incoming oceanic plate reveals an up to 600 m thick and largely undisturbed sedimentary cover; approaching the trench, however, the sediments are entirely crosscut by plate-bending faults (Figure 10). The onset of basement structures at the seafloor ~30 km seaward of the trench coincides with a vigorous decrease of crustal and upper mantle velocities. Compared to those velocity portions located 60 km south of the trench, corresponding velocities at the trench are up to 1.2 km/s lower in the mid crust and 0.6 km/s in the lower crust directly above the Moho. The oceanic crustal thickness is 9.0 km on average and hence slightly thicker than on profile 31/32. The resolved upper mantle portions reveal velocities of 7.4–7.8 km/s (see Figure 11 for data examples), which is perhaps slightly lower than corresponding velocities on profile 31/32.

[29] The plate interface is constrained by wide-angle reflections up to distances of 100 km landward of the trench down to ~22 km depth (dip: 5–8°) (Figure 10a). The boundary is of irregular shape, at least in its shallower portions, with pronounced indentations suggesting vertical displacements locally exceeding 1 km (Figure 10d). The pronounced asperity close to 105 km profile distance (Figure 10d) appears to lie in the trace of equivalent structure subducted at the western indentation of the lowermost inner-trench slope (compare Figure 2). Hence, the relief on the oceanic plate beneath the lower OAH slope may in places be associated with the subduction of inherited seafloor fabric, which is likely reactivated as response to plate bending.

[30] On this line, velocities beneath the OAH are <5.5 km/s down to ~11 km depth and thus only slightly lower than corresponding velocity portions farther north (Figure 10a). Different to the fore-arc setting observed offshore Lombok, there is only a thin sedimentary cover (no mature sedimentary basin) and crustal type velocities are observed down to ~25 km depth. Beneath the northern model edge, some steep seaward dipping reflections are observed in the wide-angle seismic data set (Figure 10b; see Figure 12 for data example). From the velocity information gained from the few rays penetrating those areas, however, it seems unlikely that this reflector is associated with a major velocity discontinuity such as the crust-mantle boundary.

4.4. Profile 21

[31] Compared to the previous lines data quality on profile 21 is only moderate, which is most likely related to the

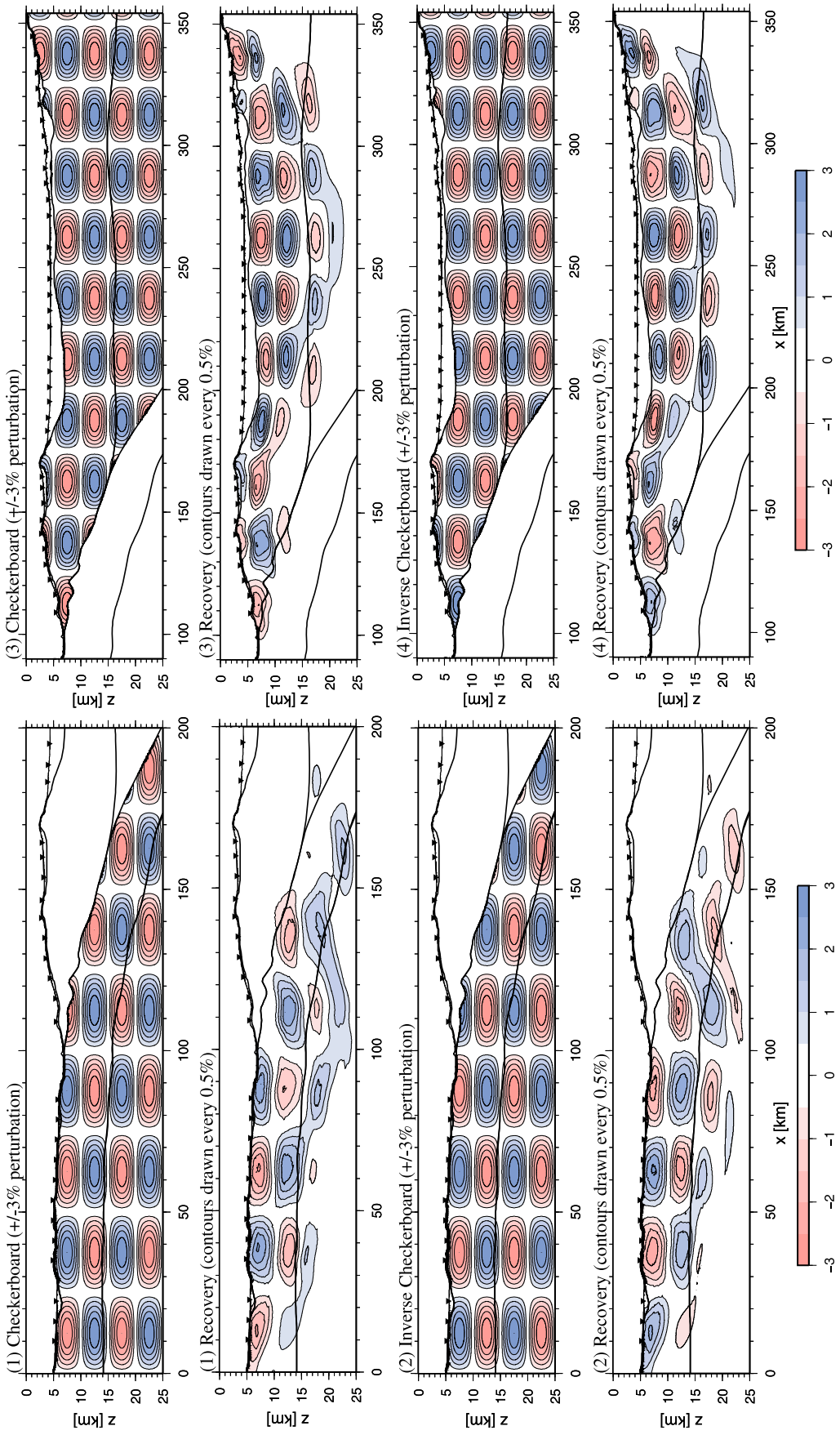

Figure 7. Resolution tests using a ±3%, 25 km × 5 km checkerboard pattern of synthetic velocity anomalies (left) within the oceanic model portions and (right) within the fore-arc model portions of profile 31/32. Tests show normal and inverse checkerboard patterns, original perturbation model and recovery after three iterations, respectively. The background model for the anomalies is the tomographic velocity model of Figure 5a. See text for discussion.

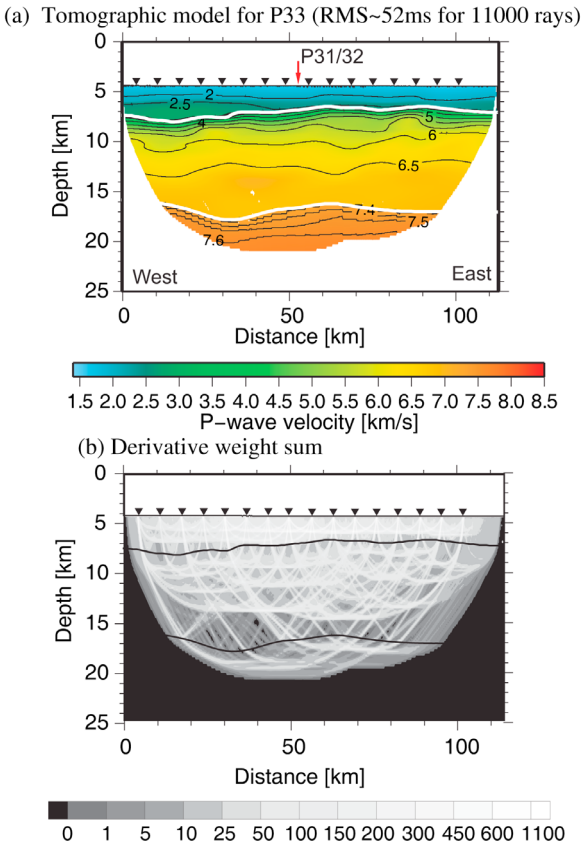

Figure 8. (a) Final tomographic velocity model of profile 33 (Lombok Basin). Triangles indicate locations of ocean bottom seismographs. Red arrow displays line intersection with profile 31/32. White lines mark structural interfaces: basement and fore-arc Moho are obtained from the joint refraction and wide-angle reflection tomography. (b) Derivative weight sum for the final tomographic velocity model.

rather complex morphology and internal structure of the OAH close to the transition to the collisional regime (see Figure 13 for data examples). The velocity model suggests significant structural changes between the western and the eastern model portions and a transition zone between ~60 km and ~100 km profile distance where the depth of the oceanic Moho increases from 19 km to 23 km (Figure 14). In the western model portions velocities reach 5.3 km/s above the plate boundary which can be traced as a continuous reflector in 11–12 km depth up to ~80 km profile distance (Figure 14b). Along the entire profile, the oceanic slab is characterized by an intracrustal reflector, which is associated with the 5.5–6.0 km/s iso-velocity line. In the eastern model portions, there is evidence for two shallower reflectors, although their continuation is sometimes unclear due to the lack of reflection coverage. If the lower reflector represents the eastern continuation of the plate boundary, this would imply a ~13 km thick subducting oceanic slab in the eastern model portions versus a 8–9 km thick slab in the western model portions (Figure 14). Accordingly, we interpret the observed change toward greater thickness of the lower plate as the transition to the collisional setting comprising the promontory of the Australian continental shelf. Resolved mantle velocities are in the range of 7.7–8.0 km/s and thus, ~0.3 km/s higher compared to corresponding velocities on profile 22 at the line intersection.

5. Gravity Data

[32] Gravity data were acquired every second using the KSS31M sea gravimeter system built by Bodenseewerk Geosystem GmbH. Using the navigation information from the ship, the measured data were corrected for the Eötvös effect and for the instrumental drift by tying it to calibrated land stations after completion of the cruise. The Free-Air Anomaly (FAA) was then obtained by subtracting the WGS67 normal gravity.

[33] We used the TOMO2D code [*Korenaga et al.*, 2001], which adopts the method of *Parker* [1973] modified by topographic correction terms, to calculate the 2-D FAA gravity response to a velocity-derived density model. For sediment, as resolved from MCS seismic data, we used the empirical velocity-density relationship $\rho = 1 + 1.18(\mathrm{Vp} - 1.5)^{0.22}$ [e.g., *Korenaga et al.*, 2000]. *Carlson and Herrick*'s [1990] conversion formula for igneous crust, $\rho = 3.81 - 6.0/\mathrm{Vp}$, was adopted for the upper oceanic crust ($\mathrm{Vp} < 6.0$ km/s) and we used a constant density of 2.90 g/cm^3 for the lower oceanic crust. Beyond the depth of seismic penetration the thickness and velocity structure of the subducting slab were held constant and its geometry was inferred from the distribution of Wadati-Benioff hypocenters [*Engdahl and Villaseñor*, 2002]. For the upper oceanic mantle we used the Vp versus ρ relationship of *Carlson and Miller* [2003], which accounts for the dependence of Vp with the degree of serpentinization and we limited the density to maximal 3.23 g/cm^3 for the deeper mantle portions.

[34] According to thermal simulations, serpentine breaks down via dehydration reactions in the subducting oceanic mantle at depths greater ~50 km (>600°C) and for old/cold slabs likely at much greater depths [*Peacock*, 2001; *Rüpke et al.*, 2004]. Hence, we expect that hydrated oceanic mantle will not recover its density by metamorphic deserpentinization reactions within the depth range of our models. We thus held constant the reduced mantle densities within the shallowmost oceanic mantle portions landward of the trench, even though Vp partly increases in our models by possible fracturing recover.

[35] For the subsequent gravity modeling we tested several models, keeping unchanged the density distribution in the oceanic crust and mantle, and changing only the densities in the overriding plates. The major aim of the applied approach is to test whether our seismically derived fore-arc geometries (mantle wedge offshore Lombok, crustal wedge offshore Sumba) can explain the gravity data reasonably well by using widely accepted velocity to density conversions.

5.1. Gravity Modeling of Profile 31/32

[36] For the overriding plate we used *Hamilton*'s [1978] relation for shale, $\rho = 0.917 + 0.747\mathrm{Vp} - 0.08\mathrm{Vp}^2$, for

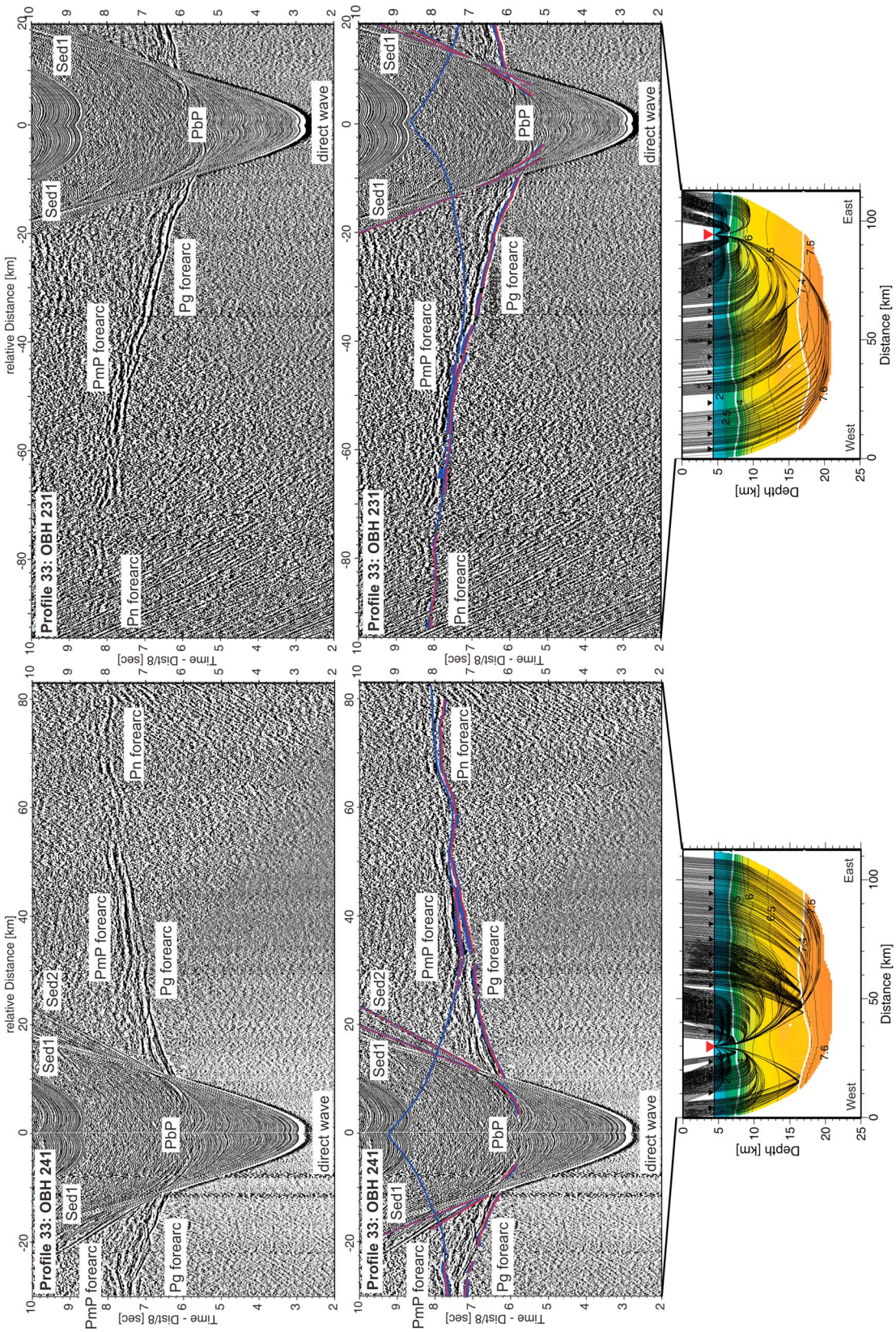

Figure 9. Seismic record sections (reduced to 8 km/s) of OBH 231 and OBH 241 on profile 33. (top) Interpreted seismic arrivals are labeled: Sed1, Sed2 (sedimentary phases), Pg fore arc (turning rays within the fore-arc crust), Pn fore arc (turning rays in the upper fore-arc mantle), PbP (reflected rays at the basement), and PmP fore arc (reflected rays at the fore-arc Moho). (middle) Picks are shown as blue bars according to their pick uncertainty, computed traveltimes are shown as red dots. Blue lines represent traveltimes for offsets not constrained by picks. (bottom) Corresponding raypaths of the picked traveltimes through the final tomographic solution of profile 33.

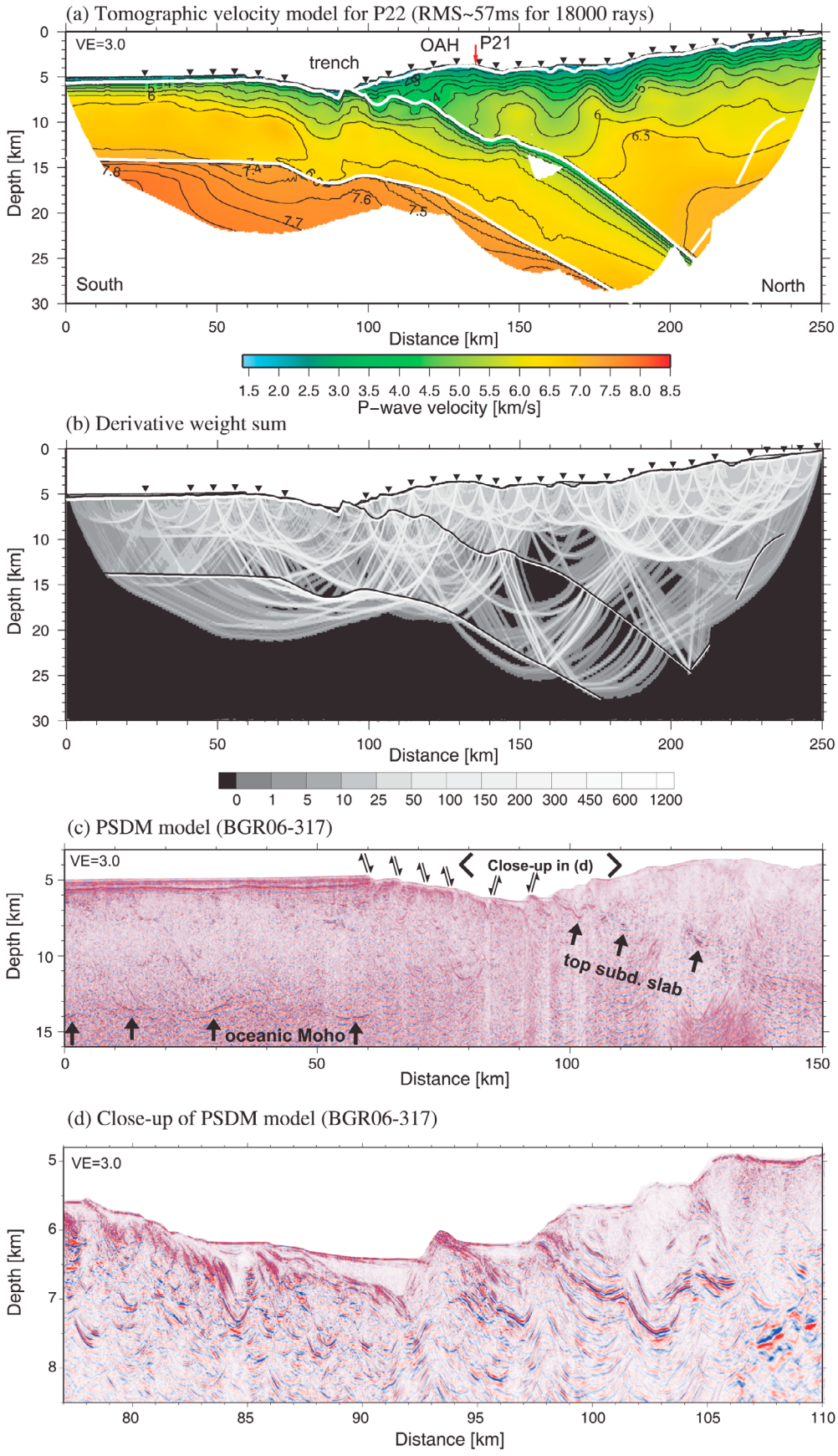
(a) Tomographic velocity model for P22 (RMS~57ms for 18000 rays)
VE=3.0
trench
OAH
P21
South
North
Depth [km]
Distance [km]
1.5 2.0 2.5 3.0 3.5 4.0 4.5 5.0 5.5 6.0 6.5 7.0 7.5 8.0 8.5
P−wave velocity [km/s]
(b) Derivative weight sum
Depth [km]
Distance [km]
0 1 5 10 25 50 100 150 200 300 450 600 1200
(c) PSDM model (BGR06-317)
VE=3.0
Close-up in (d)
top subd. slab
oceanic Moho
Depth [km]
Distance [km]
(d) Close-up of PSDM model (BGR06-317)
VE=3.0
Depth [km]
Distance [km]

Figure 10

crustal portions characterized by Vp < 5.7 km/s. We then tested three different laws for the deeper crustal portions and the fore-arc mantle (Figure 15): (1) *Carlson and Herrick*'s [1990] relation (igneous crust) and a constant mantle density of 3.20 g/cm^3, (2) *Christensen and Mooney*'s [1995] nonlinear regression for continental crustal rocks, ρ = 5.055 − 14.094/Vp, and a constant mantle density of 3.21 g/cm^3, and (3) a constant density of 2.80 g/cm^3 for the crust and the same Vp versus ρ relationship used for oceanic mantle.

[37] For the overriding plate, the relationships of *Carlson and Herrick* [1990] (igneous crust) and *Christensen and Mooney* [1995] (continental crust) yield a comparable fit by adjusting the fore-arc mantle density from 3.20 g/cm^3 to 3.21 g/cm^3 (Figure 15b). The fit is slightly improved for a model comprising a constant crustal density of 2.80 g/cm^3 and a fore-arc mantle comprising the same Vp versus ρ relationship used for oceanic mantle (Figure 15c). Thus, the gravity data is consistent with mantle alteration and a shallow fore-arc mantle, as inferred from the analysis of seismic refraction data.

5.2. Gravity Modeling of Profile 22

[38] Similar to the above described scheme we tested four different scenarios for those fore-arc portions characterized by Vp > 5.7 km/s (Figure 16): (1) a constant density of 2.75 g/cm^3 and *Birch*'s [1961] conversion law for lower crustal rocks, ρ = (Vp + 1.0)/2.67, for model portions between the intracrustal reflector and the top of the subducting slab, (2) *Carlson and Herrick*'s [1990] relationship (igneous crust) for the entire crust, (3) *Christensen and Mooney*'s [1995] relationship (continental crust) for the entire crust, and (4) a constant density of 2.80 g/cm^3 and a constant density of 2.95 g/cm^3 for model portions between the intracrustal reflector and the top of the subducting slab.

[39] The results show that a model comprising a locally lightened mantle density yields a good match to the observed gravity anomaly, again implying that the oceanic mantle beneath the trench has been altered. For the overriding plate, the relationship of *Carlson and Herrick* [1990] yields a rather poor match to the observed gravity anomaly, at least up to ~200 km profile distance (Figure 16b). Applying *Christensen and Mooney*'s [1995] conversion law (continental crust) provides a much better match to the observed data for these model portions but underpredicts the FAA anomaly for greater profile distances. Accounting for the dichotomy of the crust (upper fore arc and lower fore arc), either by using constant densities of 2.80 g/cm^3 and 2.95 g/cm^3 or by using 2.75 g/cm^3 and *Birch*'s [1961] conversion law, respectively, yield an altogether better RMS fit. However, assuming the presence of crustal-type densities beneath the steeply seaward-dipping reflector yields a good fit of the gravity data. Hence, these results are in accordance with our seismically derived model, which lacks a shallow mantle wedge offshore Sumba.

6. Discussion

6.1. Oceanic Plate and Trench

[40] A thickened oceanic crust is observed on both trench-perpendicular profiles. In case of profile 31/32, average values of 8.6 km are interpreted as the transition to the easternmost extensions of the Roo Rise and another bathymetric high near the trench close to 114.5°E (Figure 1), which locally reveal crustal thicknesses >15 km [*Curray et al.*, 1977; Shulgin et al. (submitted manuscript, 2010)]. The refraction profile offshore Lombok Strait from *Curray et al.* [1977] runs ~50 km west of profile 31/32 and reveals velocities of 8.1 km/s at 23 km depth at the trench (compared to velocities of ~7.9 km/s at ~22 km depth at the trench on profile 31/32). Owing to the large shot spacing and related difficulties in following secondary arrivals from one record to another, their evaluation of layer thickness is mainly based on the recordings of refracted arrivals, which makes their interpretation of Moho depths from these early shot records ambiguous. Hence, their depth for the 8.1 km/s velocity layer may not mark the top of the mantle, which here is constrained at ~17 km depth, but may indicate the lower limit of the observed mantle alteration.

[41] On profile 22 the crustal thickness of 9.0 km is likely related to the transition to the Scott Plateau representing the promontory of the Australian continental shelf [*Shulgin et al.*, 2009]. This is confirmed by the trench-parallel profile 21 off Sumba which suggests structural changes of the subducting crust manifested in a thickness increase of ~5 km over a distance of 40 km to the east (Figure 14). Most of the observed crustal thickening is related to the thickening of the upper crustal layer. The profile of *Shulgin et al.* [2009] at 121°E (Figure 1) reveals a 15 km thick crust beneath the Scott Plateau which seems to thin out northward when subducting beneath the Sumba Ridge. The crust shows a pronounced intracrustal reflector at roughly mid-crustal depths and is interpreted to be of continental nature. Accordingly, we interpret the easternmost portions of profile 21 as the ocean-continent transition in the subducting plate (Figure 14).

[42] Both trench-perpendicular profiles show a reduction of crustal and upper mantle velocities at distances <30–50 km seaward of the trench (Figures 5a and 10a). Obtained uppermost mantle velocities (down to ~2 km beneath the Moho) in the trench are well resolved and independent of the mantle starting model; they represent a robust feature of the tomographic inversion (please refer to Figures S1 and S2 in the auxiliary material for additional resolution tests with

Figure 10. (a) Final tomographic velocity model of profile 22. Triangles indicate locations of ocean bottom seismographs. Red arrow displays line intersection with profile 21. White lines mark structural interfaces: sedimentary portions are derived from the analysis of high-resolution MCS seismic data; plate boundary, oceanic Moho and seaward dipping intra-fore-arc reflector are obtained from the joint refraction and wide-angle reflection tomography. (b) Derivative weight sum for the final tomographic velocity model. (c) Prestack depth-migrated MCS line BGR06-317 from *Lüschen et al.* [2010]. (d) Close-up of BGR06-317. Subduction of basement asperities, located near 95 km and 105 km profile distance, results in local indentations of the deformation front (compare Figure 2). All models are plotted at 3 × vertical exaggeration. OAH, outer arc high.

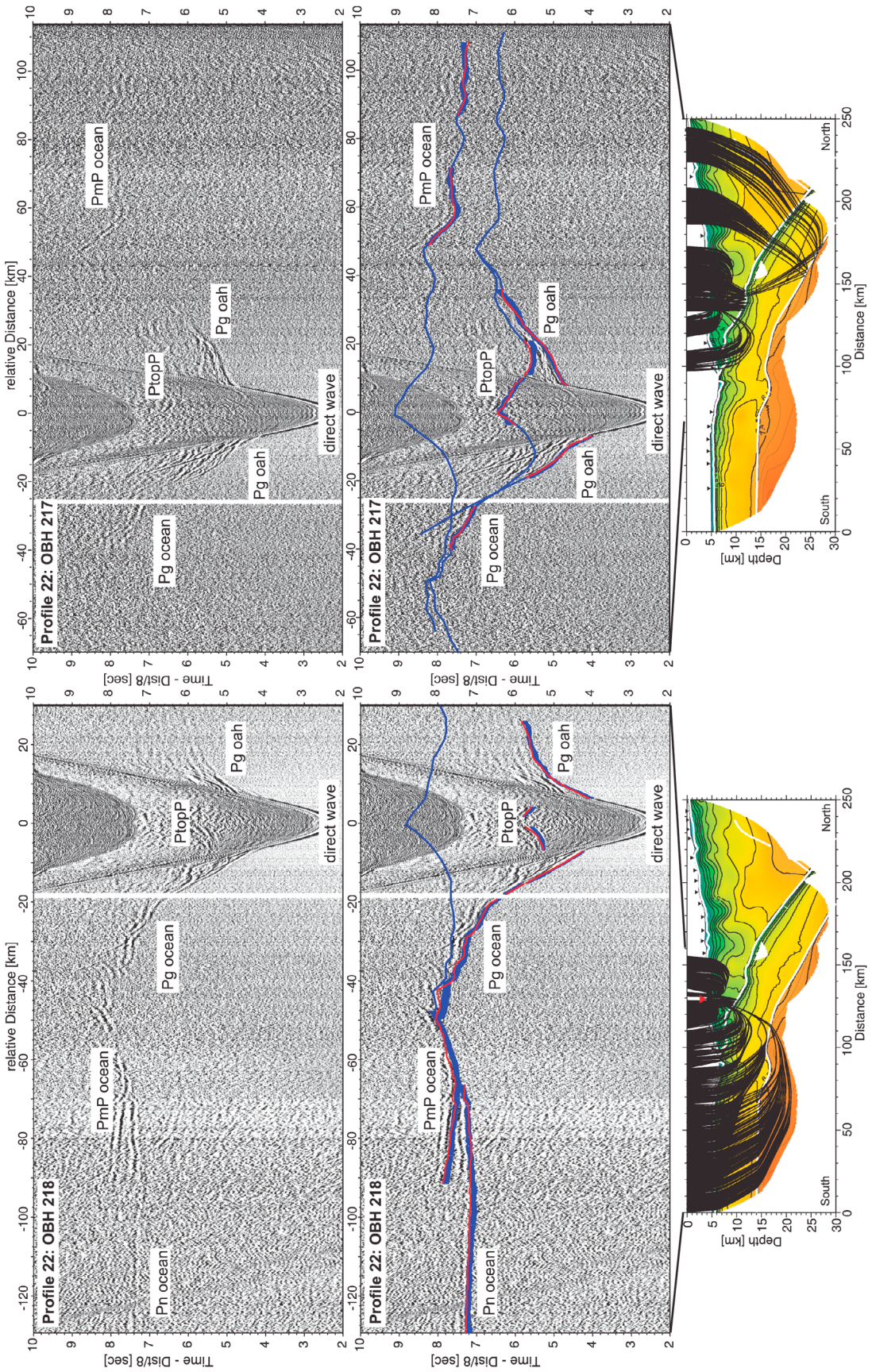

Figure 11. Seismic record sections (reduced to 8 km/s) of OBH 217 and OBH 218 on profile 22. (top) Interpreted seismic arrivals are labeled: Pg oah (turning rays within the outer arc high), Pg ocean (turning rays within oceanic crust), Pn ocean (turning rays in the upper oceanic mantle), PtopP (reflected rays at the plate interface), and PmP ocean (reflected rays at the oceanic Moho). (middle) Picks are shown as blue bars according to their pick uncertainty, computed traveltimes are shown as red dots. Blue lines represent traveltimes for offsets not constrained by picks. (bottom) Corresponding raypaths of the picked traveltimes through the final tomographic solution of profile 22.

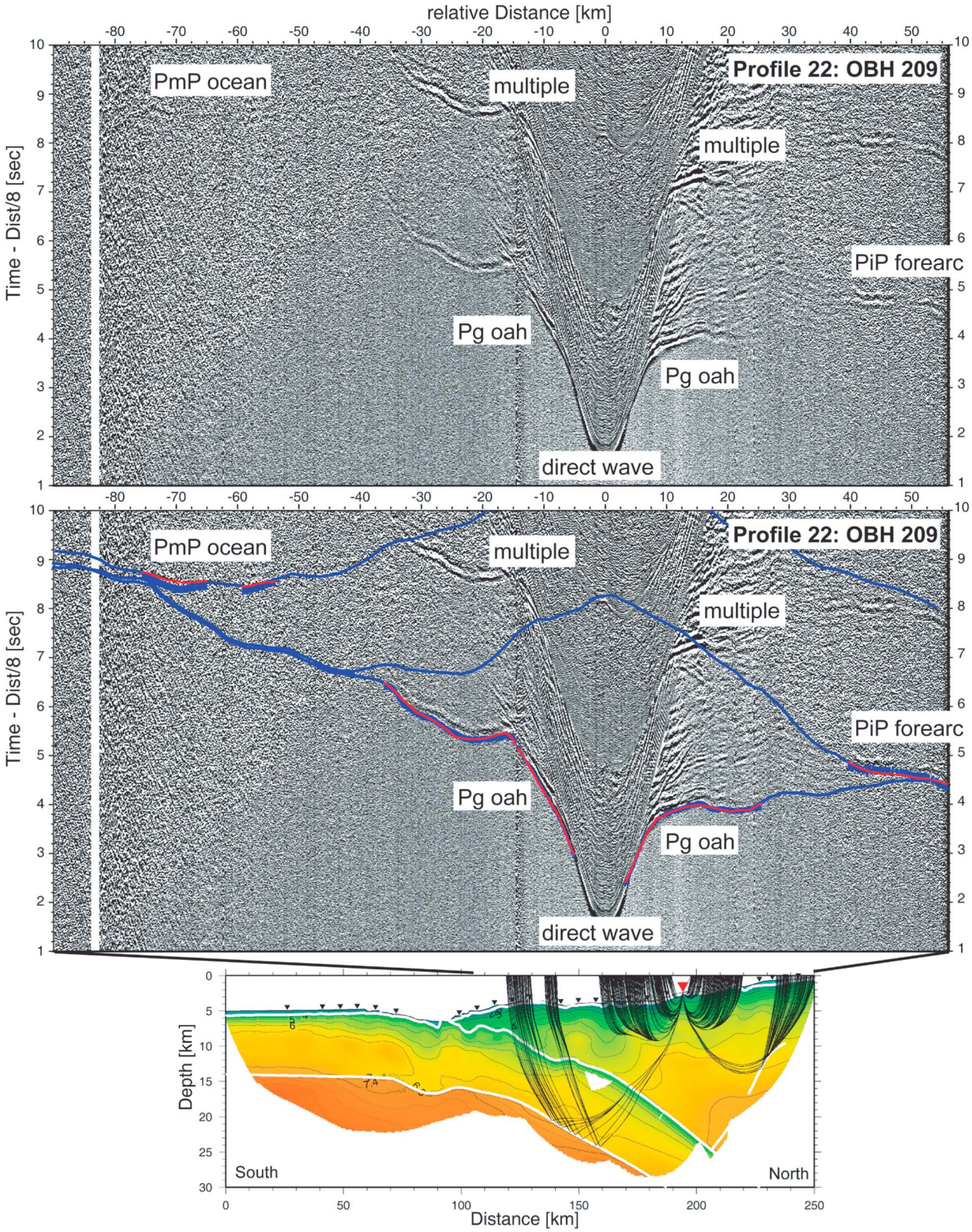

Figure 12. Seismic record section (reduced to 8 km/s) of OBH 209 on profile 22. (top) Interpreted seismic arrivals are labeled: Pg oah (turning rays within the outer arc high/fore arc), PiP fore arc (reflected rays at the intracrustal fore-arc reflector), and PmP ocean (reflected rays at the oceanic Moho). (middle) Picks are shown as blue bars according to their pick uncertainty, computed traveltimes are shown as red dots. Blue lines represent traveltimes for offsets not constrained by picks. (bottom) Corresponding raypaths of the picked traveltimes through the final tomographic solution of profile 22.

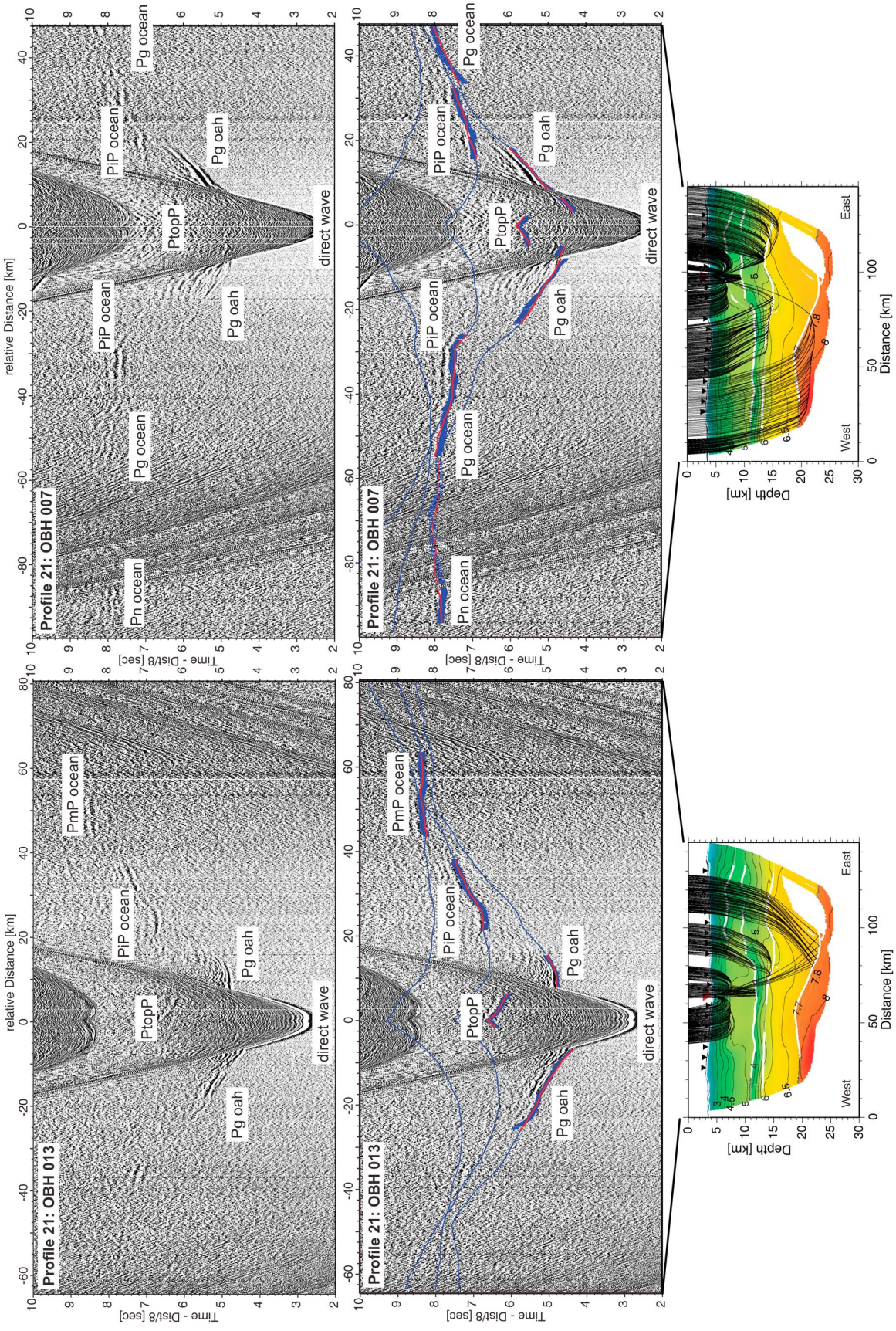
Profile 21: OBH 013
Profile 21: OBH 007
relative Distance [km]
Time - Dist/8 [sec]
PmP ocean
PiP ocean
PtopP
Pg oah
Pg ocean
Pn ocean
direct wave
Depth [km]
Distance [km]
West
East

Figure 13

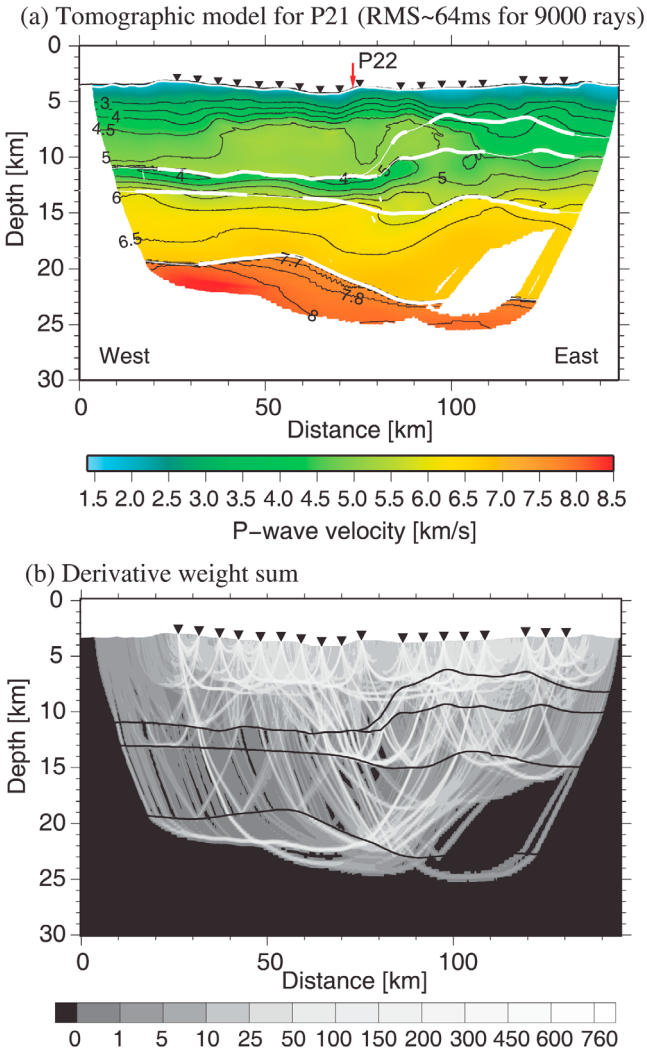

Figure 14. (a) Final tomographic velocity model of profile 21 (outer arc high). Triangles indicate locations of ocean bottom seismographs. Red arrow displays line intersection with profile 22. White lines mark structural interfaces obtained from the joint refraction and wide-angle reflection tomography (see text for details). (b) Derivative weight sum for the final tomographic velocity model.

synthetic anomalies confined to the oceanic mantle underneath the trench and an evaluation of the impact of different mantle starting models on the tomographic solution of profile 31/32). The apparent coincidence of the velocity decrease with the onset of faulting can be interpreted as the result of fracturing and subsequent alteration of the oceanic crust and serpentinization of the underlying upper mantle. Reduced upper mantle velocities within a similar range close to the trench and associated with the bending of the oceanic plate prior to subduction are found, e.g., at the Middle America trench [*Grevemeyer et al.*, 2007; *Ivandic et al.*, 2008] and offshore Chile [*Contreras-Reyes et al.*, 2007].

[43] Assuming that the velocity reduction in the upper mantle is exclusively caused by serpentinization, velocities of 7.9–7.4 km/s would imply a 0.6–2.4% increase in water content resulting in 5–19% serpentinization of mantle peridotite as a maximum estimate [*Carlson and Miller*, 2003]. However, the velocity model of profile 31/32 shows that upper mantle velocities recover to some extent from ~7.5 km/s at the trench to ~7.7 km/s beneath the lower slope of the OAH (Figure 5a; please also refer to Figure S2 of the auxiliary material). The partial recovery of mantle velocities at depths of ~20 km may indicate compressive sealing of cracks by slab-refolding and fracture-filling precipitation, because metamorphic de-serpentinization reactions occur at much greater depth during subduction of old (cold) oceanic lithosphere [*Peacock*, 2001; *Rüpke et al.*, 2004; *Faccenda et al.*, 2009]. Hence, the presence of mantle-penetrating cracks and faults likely controls the extent of the low velocity anomaly at the trench and reduces the possible degree of mantle serpentinization to probably less than 15%.

[44] On profile 22, the amplitude and intensity of the crustal low-velocity anomaly is larger and occurs more tightly confined to the trench, respectively. This is likely related to the stronger fragmentation of the oceanic crust as indicated by the greater basement relief with vertical throws of sometimes >1 km (Figure 10d). Moreover, upper mantle velocities in the uppermost 2–3 km depth beneath the Moho do not recover within the resolved model portions downdip of the trench. These observations may indicate increased tensional tectonic forces in the subducting plate.

[45] *Spence* [1986] inferred from the absence of large interface thrust earthquakes in the Sumba region, that gravitational pull of the old (dense) sinking oceanic lithosphere might have partially decoupled the subducted plate from the overriding plate. The juxtaposition of old (Late Jurassic) oceanic crust and continental crust close to ~120°E provides one of the most dramatic lateral gradients in interplate seismic coupling in the world. The combination of slab-pull on an uncoupled slab in the Java trench and the strong resistive force of the buoyant crust of the Scott Plateau to the east appears to store a tremendous amount of elastic tensile strain energy in the lithosphere at the junction of the two zones [*Spence*, 1986]. The inferred stress in the oceanic slab is transferred updip to the bending-region at the trench, leading to the 1977 Sumba earthquake, and to intense fracturing and alteration of the subducting oceanic crust and the underlying upper mantle.

6.2. Fore-Arc Offshore Lombok

[46] The most striking feature of the OAH offshore Lombok is the portion of low seismic velocities (Vp < 5.5 km/s)

Figure 13. Seismic record sections (reduced to 8 km/s) of OBH 007 and OBH 013 on profile 21. (top) Interpreted seismic arrivals are labeled: Pg oah (turning rays within the outer arc high), Pg ocean (turning rays within oceanic crust), Pn ocean (turning rays in the upper oceanic mantle), PtopP (reflected rays at the plate interface), PiP ocean (reflected rays at an intracrustal oceanic reflector), and PmP ocean (reflected rays at the oceanic Moho). (middle) Picks are shown as blue bars according to their pick uncertainty; computed traveltimes are shown as red dots. Blue lines represent traveltimes for offsets not constrained by picks. (bottom) Corresponding raypaths of the picked traveltimes through the final tomographic solution of profile 21.

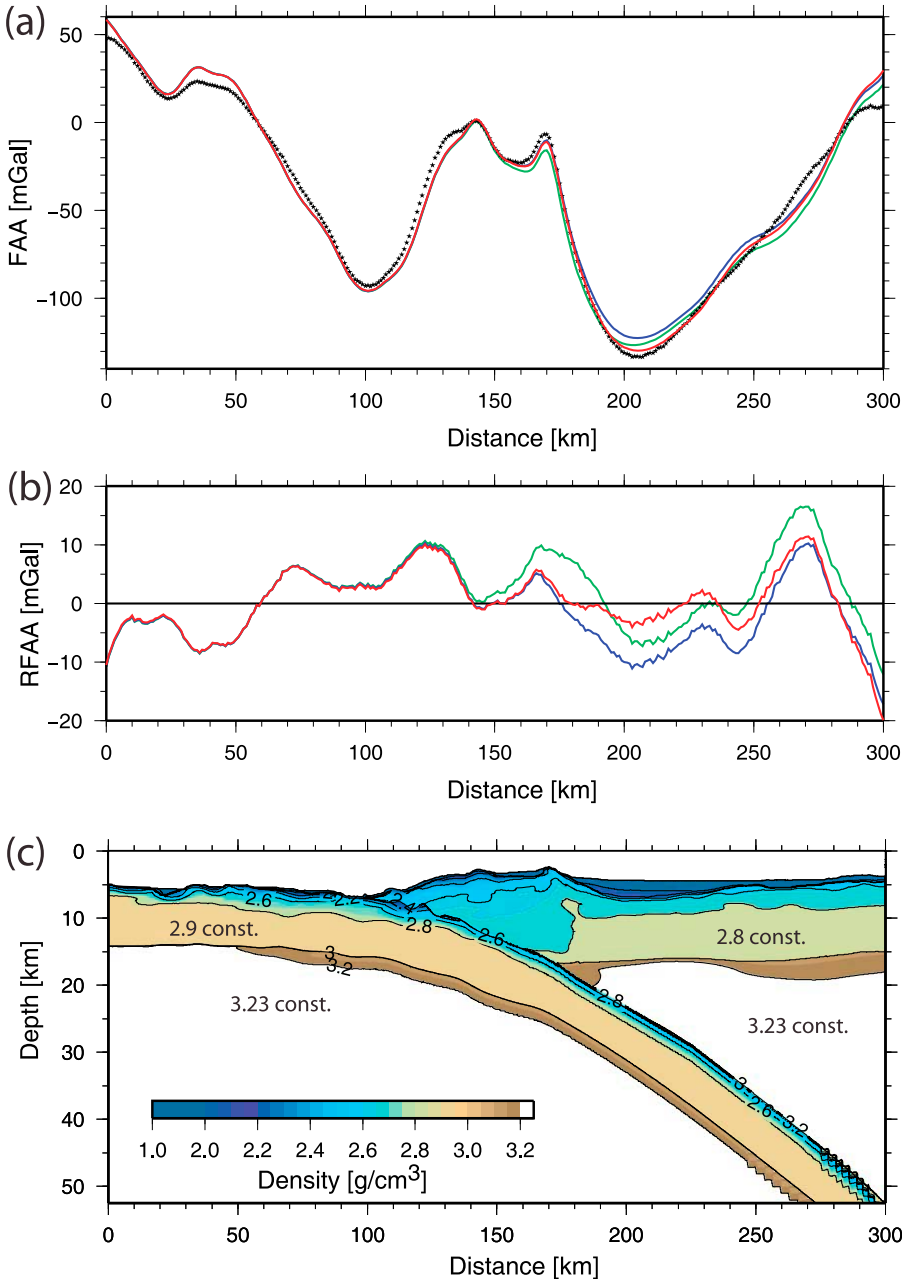

Figure 15. Gravity modeling of profile 31/32. (a) Observed free-air gravity anomaly (black points). Solid lines are from models obtained by changing overriding plate densities and keeping the same structure for oceanic crust and mantle (see text). For all calculations, *Hamilton*'s [1978] conversion law for shale is used for fore-arc portions characterized by Vp < 5.7 km/s. Blue line is for using *Carlson and Herrick*'s [1990] conversion law (igneous crust) for fore-arc crust (Vp > 5.7 km/s) and a constant fore-arc mantle density of 3.20 g/cm^3. Green line is for using *Christensen and Mooney*'s [1995] conversion law (continental crust) for fore-arc crust (Vp > 5.7 km/s) and a constant fore-arc mantle density of 3.21 g/cm^3. Red line is preferred model shown in Figure 15c. (b) Residual free-air gravity anomaly (RFAA) obtained by subtracting calculated from observed anomaly. Model with *Carlson and Herrick*'s [1990] conversion law has RMS of 6.5 mGal (blue line). Model with *Christensen and Mooney*'s [1995] conversion law has RMS of 6.2 mGal (green line). Preferred model has RMS of 5.7 mGal (red line). (c) Preferred density model using a constant density of 2.8 g/cm^3 for fore-arc crust (Vp > 5.7 km/s) and *Carlson and Miller*'s [2003] conversion law for both the oceanic and fore-arc mantle (restricted to maximal 3.23 g/cm^3).

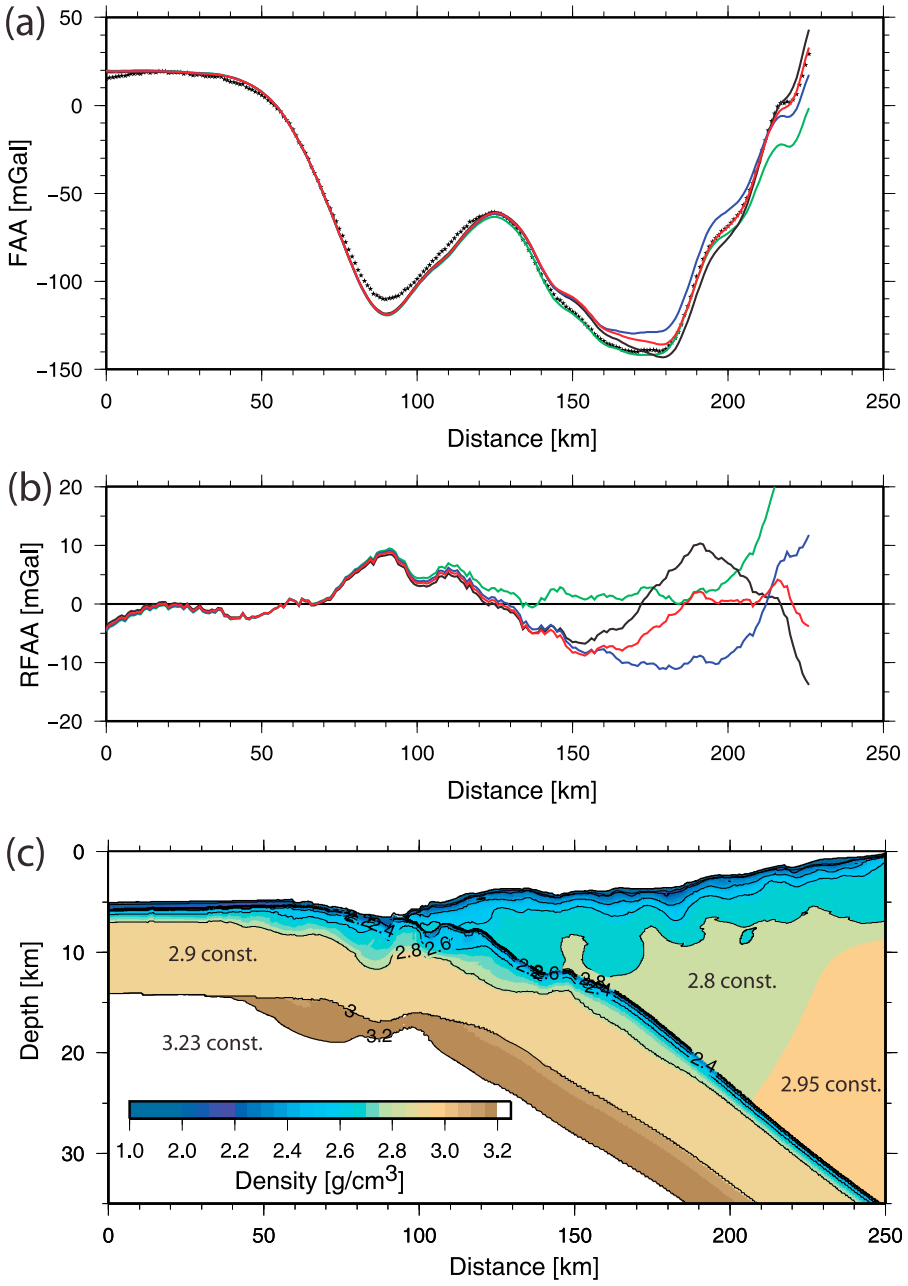

Figure 16. Gravity modeling of profile 22. (a) Observed free-air gravity anomaly (black points). Solid lines are from models obtained by changing overriding plate densities and keeping the same structure for oceanic crust and mantle (see text). For all calculations, *Hamilton*'s [1978] conversion law for shale is used for fore-arc portions characterized by Vp < 5.7 km/s. Black line is for using a constant density of 2.75 g/cm^3 for the upper fore arc (Vp > 5.7 km/s) and *Birch*'s [1961] conversion law (lower crust) for the lower fore arc between intracrustal reflector and top of subducting slab. Blue line is for using *Carlson and Herrick*'s [1990] conversion law (oceanic crust), restricted to maximal 2.9 g/cm^3, for the entire fore arc (Vp > 5.7 km/s). Green line is for using *Christensen and Mooney*'s [1995] conversion law (continental crust), restricted to maximal 2.9 g/cm^3, for the entire fore arc (Vp > 5.7 km/s). Red line is preferred model shown in Figure 16c. (b) Residual free-air gravity anomaly (RFAA) obtained by subtracting calculated from observed anomaly. Model with *Carlson and Herrick*'s [1990] conversion law has RMS of 6.4 mGal (blue line). Model with *Christensen and Mooney*'s [1995] conversion law has RMS of 5.8 mGal (green line). Model with *Birch*'s [1961] conversion law for the lower fore arc has RMS of 4.5 mGal (black line). Preferred model has RMS of 4.0 mGal (red line). (c) Preferred density model using a constant density of 2.8 g/cm^3 for the upper fore arc (Vp > 5.7 km/s) and 2.95 g/cm^3 for the lower fore arc between intracrustal reflector and top of subducting slab.

down to the plate interface (down to ~13 km depth), which points toward a sedimentary rock origin of this feature (Figure 5). On the lowermost inner trench slope (>5 km depth) profile 31/32 suggests the presence of a frontal prism, which displays low seismic velocities (Vp~3 km/s) and originates from frontal accretion of trench sediments. The MCS profile draws only one imbricate thrust sheet (Figure 6), probably due to local indentations of the trench, but more than three arrays of thrust ridges appear at the seafloor farther to the east (Figure 2).

[47] Currently, only moderate sedimentary portions are involved in the formation of the OAH, comprising mainly the thin (<600 m) predominantly pelagic sedimentary cover visible atop the oceanic plate and some turbidites and slump deposits from the inner trench slope [*Lüschen et al.*, 2010]. A possible sediment supply from the fore arc is blocked due to the higher elevation of the OAH representing an effective barrier from the depocenters of the Lombok Basin. However, taking into account the ~25 Ma long period of subduction at the eastern Sunda Arc [e.g., *Hall and Smyth*, 2008], continuous accretion of sediment could have formed major portions of the OAH although involved sedimentary volumes are moderate [*Van der Werff*, 1995].

[48] Sediment supply may have been more abundant before the approach of the Roo Rise to the trench. Off eastern Java, the onset of subduction of the Roo Rise resulted in an uplift of the trench and subsequent truncation of sediment supply from the Bengal Fan. At present, however, only ~1.5 km sediment thickness are trapped west of this barrier in the trench off western Java [*Kopp et al.*, 2002], which suggests little effects on trench sediment contribution off Lombok and farther east.

[49] Beneath the higher elevated OAH portions the MCS seismic profile of *Lüschen et al.* [2010] displays a number of landward dipping faults associated with a prominent slope break and with the system of tectonic ridges and the small basin in between (Figure 6). This morphological array of ridges and piggyback basins in between correlates with similar structures farther west, where these features are associated with landward dipping splay faults [*Müller et al.*, 2008; *Lüschen et al.*, 2010]. Offshore Lombok, at least two faults seem to penetrate the entire OAH and connect to the plate interface (Figure 6). The higher-elevated OAH portions display only minimal reflectivity. Hence, from the available data it is difficult to judge whether these faults are "out of sequence" splay faults or reactivated imbricate thrust faults which are shortened and steepened due to compression.

[50] Profile 31/32 reveals a sharp lateral increase of crustal velocities beneath the landward slope break of the OAH suggesting distinct lithological changes associated with the transition from the northern ridge to those fore-arc portions capped by the sedimentary strata comprising the Lombok Basin (Figure 5). Crustal velocities beneath the basin rapidly increase to 5.5–6.0 km/s and then rise somewhat more gentle to ~6.8 km/s above the upper plate Moho. A similar lateral velocity change from 4.0 km/s to 5.5 km/s is observed offshore Chile at the transition from the outer rise to the Valparaiso Basin and is interpreted as a lithological transition from accreted sediment to continental margin framework [*Flueh et al.*, 1998]. On profile 31/32, there is a portion of high velocities, located at 7–10 km depth and ~180 km profile distance, which are bounded by landward dipping reflections (Figure 6). The observed structure could be interpreted as the tip of the basement of the Lombok Basin, which was tilted and lifted up by underthrusting along with the thickening of sediments during OAH generation. Such architectures are common in ancient accretionary terranes exposed on land [*Dickinson and Seely*, 1979]. The uplift and northward tilt of the basement beneath the northern ridge and the seismic facies of the Lombok Basin crust distinct from the OAH may be suggestive for an arcward dipping backstop located beneath the landward slope break of the OAH. On a magnetic profile crossing the OAH this transition is marked by a sharp negative anomaly (~40 km wide, −300 nT amplitude), which might result from a package of steeply inclined tectonically accreted volcanic sills [*Mueller and Neben*, 2006]. Results from the analysis of MCS data show an irregular topography of the Lombok fore-arc basement reminiscent of horst and graben structures at rifted continental margins or stacked ophiolite sheets and nappes, which could be formed by underthrusting of younger oceanic blocks and subsequent steepening due to continuous compression [*Lüschen et al.*, 2010].

[51] The thickness of the fore-arc crust on profile 31/32 ranges from 9 km beneath the portions of highest sedimentary infill to 11 km at ~250 km profile distance (Figure 5). There is no distinct lateral change in crustal velocities in the northernmost model portions, but crustal thickness likely increases to >14 km here. A high velocity lower crust (6.8–7.2 km/s), which represents about 30% of the total crust of the subducting oceanic plate, is lacking in the fore-arc crust, resulting in an average crustal velocity (considering crustal velocity portions characterized by $Vp > 6.0$ km/s) of 6.51 ± 0.07 km/s compared to 6.71 ± 0.09 km/s for the subducting plate. From the distribution of zircon ages in sedimentary and igneous rocks from southeast Java, *Smyth et al.* [2007] infer the presence of a Gondwana continental fragment from northwest Australia, which was accreted offshore East Java in the Late Cretaceous; the eastern extent of this fragment is unknown but the oceanic type velocity structure beneath the Lombok Basin rather precludes a possible continuation into this area.

[52] The fore-arc crust in our models could be interpreted as an altered, heavily fractured piece of an older oceanic terrane, perhaps formed during the opening of the Indian Ocean during Cretaceous to middle Eocene times, which was hindered from subduction due to its increased buoyancy; a similar scenario was previously invoked to explain the origin of the fore arc offshore Lombok Strait [*Curray et al.*, 1977] and western Java [*Kopp et al.*, 2002]. The relatively constant crustal velocity of the fore-arc basement may imply a distinct change in lithological composition toward the volcanic arc, unless the arc massif is composed mainly of oceanic crust or ophiolite as the fore-arc basement. The base of the fore-arc basement marks the crust mantle boundary, as the seismic and gravity data strongly support the presence of shallow mantle material here.

[53] The uppermost mantle offshore Lombok exhibits rather low velocities (7.4–7.8 km/s). Similar velocity structures are observed beneath the Izu-Bonin intraoceanic arc and are interpreted as "Moho transition zone" comprising mafic restite and cumulatives resulting from processes of anatexis and magmatic differentiation of the mafic and ultramafic crustal components [*Tatsumi et al.*, 2008; *Kodaira et al.*, 2008]. In order to invoke analogous processes beneath the

fore arc offshore Lombok, this scenario would imply the presence of a paleoarc ~100 km south of the present volcanic front near 250–300 km profile distance on line 31/32, where the velocity reduction in the upper mantle appears to be enhanced. In East Java a paleoarc, which was active from Eocene to early Miocene times, is located ~50 km south of the current volcanic front [*Smyth et al.*, 2008; *Hall and Smyth*, 2008]. The coincident magnetic profile of line 31/32 shows a generally smooth magnetic field across the Lombok Basin, but beginning with ~265 km profile distance displays magnetic anomalies of ±100 nT [*Mueller and Neben*, 2006], which would correspond to the location of enhanced velocity reduction in the upper mantle and thus to the inferred origin of this structure from a possible paleovolcanic arc.

[54] However, the strong Moho reflection associated with the top of the 7.4–7.8 km/s layer beneath the Lombok Basin (see Figures 4 and 9) argues for a distinct lithological boundary rather than a "chemically transparent" Moho located within the mafic restite/cumulate layer. In this alternative scenario, sub-fore-arc water release from subducted sediment and crust facilitates a significant degree of mantle serpentinization (up to 19% according to the Vp relationship of *Carlson and Miller* [2003]) [*Bostock et al.*, 2002; *Hyndman and Peacock*, 2003; *Rüpke et al.*, 2004].

[55] The presence of a shallow mantle wedge off Java was already proposed by *Kopp et al.* [2002, 2009] based on seismic wide-angle and refraction data, and a possible continuation farther east of this feature was suggested by *Grevemeyer and Tiwari* [2006] on the basis of gravity modeling. The profile of *Curray et al.* [1977] conducted ~50 km west of profile 31/32 shows a fore-arc Moho at ~18 km depth and upper mantle velocities of 7.8–8.4 km/s in the fore arc off the Lombok Strait. Hence, their Moho depths are ~2 km deeper and observed mantle velocities are 0.4–0.6 km/s higher than the results of this study (compare discussion of the results of *Curray et al.* [1977] in section 6.1).

[56] *Oleskevich et al.* [1999] suggest that the downdip limit and thus the width of the seismogenic coupling zone, which controls the potential magnitude of large megathrust earthquakes, is governed by the depth of the intersection of the thrust with the fore-arc mantle and the presence of weak hydrous minerals in the mantle wedge, which do not support seismogenic stick-slip behavior. Offshore Java a shallow serpentinized mantle wedge underlying the fore-arc basin would limit the width of the coupling zone to only 30–40 km, compared to >120 km offshore Sumatra [*Grevemeyer and Tiwari*, 2006]. Thermal modeling shows that the updip limit of the seismogenic zone (~100°C isotherm [*Hyndman and Wang*, 1993]) offshore Java is located ~80 km landward from the trench [*Grevemeyer and Tiwari*, 2006]. Offshore Lombok, the similar trench-normal convergence rate and dip but the older age of the subducting plate suggest a thermally defined updip limit that reaches farther landward from the trench and thus, the width of the seismogenic coupling zone is likely to be even narrower here. The distribution of earthquake hypocenters off Lombok and Sumbawa shows a band of extensional mechanisms closely confined to the trench and some events revealing compressional mechanisms beneath the fore-arc basin and the volcanic arc [*Špičák et al.*, 2007]. The OAH belongs to a >100 km wide zone in between characterized by virtually no teleseismically recorded earthquakes related to the plate boundary (down to a regional threshold magnitude of ~5.5) [e.g., *Engdahl and Villaseñor*, 2002]. These observations strongly contrast with the adjacent Sumatra-Andaman margin segment where the recent and historic earthquake record suggests a much larger potential for destructive subduction zone megathrust earthquakes than for Java and Lombok [*Lay et al.*, 2005; *Newcomb and McCann*, 1987]. Thus, the shallow serpentinized mantle wedge, which is absent offshore Sumatra [*Kieckhefer et al.*, 1980; *Kopp et al.*, 2002], might be the major factor limiting the magnitude of rupture offshore Java and Lombok. The system of possible splay faults in the outer arc high, however, demonstrates that potential movements can be transmitted to shallow seafloor portions and thus, this margin is nevertheless prone to a serious tsunami hazard [*Müller et al.*, 2008; *Kopp et al.*, 2009; *Lüschen et al.*, 2010] (Figure 6).

6.3. Fore-Arc Offshore Sumba

[57] The strong relief of the plate boundary imaged in both the wide-angle and MCS seismic data suggests significant vertical steps between dissected oceanic blocks, probably further increased due to plate bending during subduction (Figure 10d). Where these asperities subduct beneath the trench they entrain lower slope material and cause slope failure in their wake (see slide in Figure 2) and thus, may unbalance the mass budget along this margin segment toward local erosion of the frontal prism.

[58] Contrary to the geometry offshore Lombok, the similar velocity structure of the OAH and the adjacent fore-arc portions farther north may imply similar constituents (Figure 10). Velocities in the northern fore-arc portions suggest a greater heterogeneity and related vertical velocity gradients are lower (velocities do not reach 6 km/s within the uppermost 6–10 km beneath the basement, compared to ~5 km on profile 31/32). In our models the base of this unit is marked by the steep seaward dipping reflector identified in the wide-angle seismic data. The seismic refraction data, however, do not support the presence of mantle velocities directly below this reflector and the gravity data go conform with the presence of crustal-type densities between the reflector and the plate interface (Figure 16). We interpret this deeper unit as the westward extension of the crystalline basement beneath the Sumba Ridge in the seismic profile of *Shulgin et al.* [2009] at 121°E and eventually as the onset of the "Sumba block" [e.g., *Rutherford et al.*, 2001]. In the structural interpretation of *Shulgin et al.* [2009], the seaward dipping interface separates the paleoaccretionary prism from the Sumba Ridge crust, which extends down to the crust-mantle boundary at 26–28 km depth. Hence, these models do not support the presence of a shallow mantle wedge south and east of the island of Sumba.

7. Conclusions

[59] The combined analysis of seismic wide-angle reflection and refraction data, multichannel streamer data and shipboard gravity data, reveals the velocity and density structure of the incoming oceanic plate and the overriding plate offshore Lombok and offshore Sumba at the transition to the collisional regime farther east.

[60] 1. Offshore Lombok, the incoming oceanic crust is on average 8.6 km thick and largely devoid of sediment.

Seismic velocities in the crust and in the uppermost mantle are reduced within 40 km seaward of the trench, which coincides with the onset of normal faulting in the bathymetry and MCS seismic data. Velocities of 7.4–7.9 km/s in the uppermost ~2 km beneath the Moho suggest the presence of mantle-penetrating cracks and faults as well as significant degrees of mantle serpentinization.

[61] 2. Velocities in the outer arc high rarely exceed 5.5 km/s down to the top of the subducting slab, which is traced over at least 70 km beneath the fore arc down to ~15 km depth. These bulk velocities are characteristic of an accretionary origin, with highly compacted sediments (possibly partially metamorphosed) at depth. The complex shape of the plate boundary in our models indicates a highly fractured oceanic crust.

[62] 3. In the Lombok Basin up to 3.7 km of sedimentary strata overlies a 9–11 km thick crust which is characterized by an oceanic type velocity structure. Velocities of 7.4–7.8 km/s beneath a distinct Moho reflector suggest a hydrated mantle wedge at ~16 km depth beneath the Lombok Basin, which is also supported by the gravity modeling for this corridor. Because serpentinites are expected at shallow depths in the mantle wedge, they may control, at least partially, the seismological stick-slip behavior of the megathrust; in particular, they may reduce the width of the seismic coupling zone and thus limit the potential magnitude of large subduction megathrust earthquakes offshore Lombok. The system of possible splay faults in the outer arc high, however, demonstrates that potential movements can be transmitted to shallow seafloor portions and thus poses a serious tsunami threat for this margin.

[63] 4. Offshore Sumba, the oceanic crust is on average 9.0 km thick and at greater distance from the trench comprises a thin (<600 m) largely undisturbed sedimentary cover. Within 30 km seawards of the trench, intense fracturing of the crust coincides with a vigorous decrease of crustal velocities. Here, upper mantle velocities reach 7.4–7.8 km/s. If the adjacent Scott Plateau resists to be subducted, pervasive rupture of the oceanic crust and subsequent serpentinization of the underlying mantle may be the effect of increased tensional tectonic forces due to sustained slab-pull.

[64] 5. Slope indentations and the presence of fan-shaped slide deposits in the trench suggest that subduction of pronounced seafloor asperities, including reactivated seafloor fabric and plate-bending faults, locally contribute to the frontal erosion of the lower slope.

[65] 6. From west to east the subducting slab thickens from ~9 km to ~13 km beneath the outer arc high, which we interpret as the transition from the oceanic crust of the Argo Abyssal Plain to the promontory of the Australian continental shelf comprising the Scott Plateau.

[66] 7. Our seismic and gravity models do not support the presence of a shallow mantle wedge beneath the fore arc. A steep seaward dipping reflector in the northernmost model portions of profile 22 may be related to the transition to the "Sumba block" farther north.

[67] **Acknowledgments.** This paper benefited from the constructive reviews by H. Ueda and an anonymous reviewer. The SINDBAD project was funded by the German Federal Ministry of Education and Research (BMBF) under grants 03G0190A and 03G0190B. We would like to thank the master and crew of R/V *Sonne* for their professional assistance during cruise SO190 and the SINDBAD scientific party for their enormous help during data acquisition.

References

Bialas, J., and E. R. Flueh (1999), Ocean bottom seismometers, *Sea Technol.*, *40*(4), 41–46.

Birch, F. (1961), The velocity of compressional waves in rocks to 10 kilobars, *J. Geophys. Res.*, *66*, 2199–2224, doi:10.1029/JZ066i007p02199.

Bock, Y., L. Prawirodirdjo, J. F. Genrich, C. W. Stevens, R. McCaffrey, C. Subarya, S. S. O. Puntodewo, and E. Calais (2003), Crustal motion in Indonesia from Global Positioning System measurements, *J. Geophys. Res.*, *108*(B8), 2367, doi:10.1029/2001JB000324.

Bostock, M. G., R. D. Hyndman, S. Rondenay, and S. M. Peacock (2002), An inverted continental Moho and the serpentinization of the forearc mantle, *Nature*, *417*, 536–538, doi:10.1038/417536a.

Carlson, R. L., and C. N. Herrick (1990), Densities and porosities in the oceanic crust and their variations with depth and age, *J. Geophys. Res.*, *95*(B6), 9153–9170, doi:10.1029/JB095iB06p09153.

Carlson, R. L., and D. J. Miller (2003), Mantle wedge water contents estimated from seismic velocities in partially serpentinized peridotites, *Geophys. Res. Lett.*, *30*(5), 1250, doi:10.1029/2002GL016600.

Christensen, N. I., and W. D. Mooney (1995), Seismic velocity structure and composition of the continental crust: A global view, *J. Geophys. Res.*, *100*(B6), 9761–9788, doi:10.1029/95JB00259.

Clift, P., and P. Vannucchi (2004), Controls on tectonic accretion versus erosion in subduction zones: Implications for the origin and recycling of the continental crust, *Rev. Geophys.*, *42*, RG2001, doi:10.1029/2003RG000127.

Curray, J. R., G. S. Shor, R. W. Raitt, and M. Henry (1977), Seismic refraction and reflection studies of crustal structure of the eastern Sunda and western Banda arcs, *J. Geophys. Res.*, *82*, 2479–2489, doi:10.1029/JB082i017p02479.

Collot, J.-Y., W. Agudelo, A. Ribodetti, and B. Marcaillou (2008), Origin of a crustal splay fault and its relation to the seismogenic zone and underplating at the erosional north Ecuador–south Colombia oceanic margin, *J. Geophys. Res.*, *113*, B12102, doi:10.1029/2008JB005691.

Contreras-Reyes, E., I. Grevemeyer, E. R. Flueh, M. Scherwath, and M. Heesemann (2007), Alteration of the subducting oceanic lithosphere at the southern central Chile trench–outer rise, *Geochem. Geophys. Geosyst.*, *8*, Q07003, doi:10.1029/2007GC001632.

Dickinson, W. R., and D. R. Seeley (1979), Structure and stratigraphy of forearc regions, *AAPG Bull.*, *63*, 2–31.

Engdahl, E. R., and A. Villaseñor (2002), Global seismicity: 1900–1999, in *International Handbook of Earthquake and Engineering Seismology*, edited by W. H. K. Lee et al., pp. 665–690, doi:10.1016/S0074-6142(02)80244-3, Academic, Amsterdam.

Faccenda, M., T. V. Taras, and L. Burlini (2009), Deep slab hydration induced by bending-related variations in tectonic pressure, *Nat. Geosci.*, *2*, 790–793, doi:10.1038/ngeo656.

Flueh, E. R., N. Vidal, C. R. Ranero, A. Hoijka, R. von Huene, J. Bialas, K. Hinz, D. Cordoba, J. J. Danobeitia, and C. Zelt (1998), Seismic investigations of the continental margin off- and onshore Valparaiso, Chile, *Tectonophysics*, *288*, 251–263, doi:10.1016/S0040-1951(97)00299-0.

Grevemeyer, I., and V. M. Tiwari (2006), Overriding plate controls spatial distribution of megathrust earthquakes in the Sunda–Andaman subduction zone, *Earth Planet. Sci. Lett.*, *251*(3–4), 199–208, doi:10.1016/j.epsl.2006.08.021.

Grevemeyer, I., C. R. Ranero, E. R. Flueh, D. Klaeschen, and J. Bialas (2007), Passive and active seismological study of bending-related faulting and mantle serpentinization at the Middle America trench, *Earth Planet. Sci. Lett.*, *258*, 528–542, doi:10.1016/j.epsl.2007.04.013.

Hall, R. (2002), Cenozoic geological and plate tectonic evolution of SE Asia and the SW Pacific: Computer-based reconstructions, model and animations, *J. Asian Earth Sci.*, *20*, 353–431, doi:10.1016/S1367-9120(01)00069-4.

Hall, R., and H. R. Smyth (2008), Cenozoic arc processes in Indonesia: Identification of the key influences on the stratigraphic record in active volcanic arcs, in *Formation and Applications of the Sedimentary Record in Arc Collision Zones*, edited by A. E. Draut, P. D. Clift, and D. W. Scholl, *Spec. Pap. Geol. Soc. Am.*, 436, 27–54, doi:10.1130/2008.2436(03).

Hamilton, E. L. (1978), Sound velocity–density relations in sea-floor sediment and rocks, *J. Acoust. Soc. Am.*, *63*(2), 366–377, doi:10.1121/1.381747.

Hamilton, W. B. (1988), Plate tectonics and island arcs, *Geol. Soc. Am. Bull.*, *100*, 1503–1527, doi:10.1130/0016-7606(1988)100<1503:PTAIA>2.3.CO;2.

Heine, C., R. D. Mueller, and C. Gaina (2004), Reconstructing the lost Tethys Ocean basin: Convergence history of the SE Asian margin and marine gateways, in *Continent-Ocean Interactions Within East Asian Marginal Seas*, *Geophys. Monogr. Ser.*, vol. 149, edited by P. Clift et al., pp. 37–54, AGU, Washington, D. C.

Heirtzler, J. R., et al. (1974), Site 261, *Initial Rep. Deep Sea Drill. Proj.*, *27*, 129–192.

Hyndman, R. D., and S. M. Peacock (2003), Serpentinization of the forearc mantle, *Earth Planet. Sci. Lett.*, *212*, 417–432, doi:10.1016/S0012-821X(03)00263-2.

Hyndman, R. D., and K. Wang (1993), Thermal constraints on the zone of major thrust earthquake failure: The Cascadia subduction zone, *J. Geophys. Res.*, *98*, 2039–2060, doi:10.1029/92JB02279.

Ivandic, M., I. Grevemeyer, A. Berhorst, E. R. Flueh, and K. McIntosh (2008), Impact of bending related faulting on the seismic properties of the incoming oceanic plate offshore of Nicaragua, *J. Geophys. Res.*, *113*, B05410, doi:10.1029/2007JB005291.

Kieckhefer, R. M., G. G. Shor Jr., J. R. Curray, W. Sugiarta, and F. Hehuwat (1980), Seismic refraction studies of the Sunda Trench and forearc basin, *J. Geophys. Res.*, *85*, 863–889, doi:10.1029/JB085iB02p00863.

Kodaira, S., T. Sato, N. Takahashi, M. Yamashita, T. No, and Y. Kaneda (2008), Seismic imaging of a possible paleoarc in the Izu-Bonin intraoceanic arc and its implications for arc evolution processes, *Geochem. Geophys. Geosyst.*, *9*, Q10X01, doi:10.1029/2008GC002073.

Kopp, H., and N. Kukowski (2003), Backstop geometry and accretionary mechanics of the Sunda margin, *Tectonics*, *22*(6), 1072, doi:10.1029/2002TC001420.

Kopp, H., E. R. Flueh, D. Klaeschen, J. Bialas, and C. Reichert (2001), Crustal structure of the central Sunda margin at the onset of oblique subduction, *Geophys. J. Int.*, *147*, 449–474, doi:10.1046/j.0956-540x.2001.01547.x.

Kopp, H., D. Klaeschen, E. R. Flueh, J. Bialas, and C. Reichert (2002), Crustal structure of the Java margin from seismic wide-angle and multichannel reflection data, *J. Geophys. Res.*, *107*(B2), 2034, doi:10.1029/2000JB000095.

Kopp, H., E. R. Flueh, C. J. Petersen, W. Weinrebe, A. Wittwer, and Meramex Scientists (2006), The Java margin revisited: Evidence for subduction erosion off Java, *Earth Planet. Sci. Lett.*, *242*, 130–142, doi:10.1016/j.epsl.2005.11.036.

Kopp, H., D. Hindle, D. Klaeschen, O. Oncken, C. Reichert, and D. Scholl (2009), Anatomy of the western Java plate interface from depth-migrated seismic images, *Earth Planet. Sci. Lett.*, *288*, 399–407, doi:10.1016/j.epsl.2009.09.043.

Korenaga, J., W. Holbrook, G. Kent, P. Kelemen, R. Detrick, H.-C. Larsen, J. Hopper, and T. Dahl-Jensen (2000), Crustal structure of the southeast Greenland margin from joint refraction and reflection seismic tomography, *J. Geophys. Res.*, *105*(B9), 21,591–21,614, doi:10.1029/2000JB900188.

Korenaga, J., W. S. Holbrook, R. S. Detrick, and P. B. Kelemen (2001), Gravity anomalies and crustal structure across the southeast Greenland margin, *J. Geophys. Res.*, *106*, 8853–8870, doi:10.1029/2000JB900416.

Lay, T., et al. (2005), The Great Sumatra-Andaman earthquake of 26 December 2004, *Science*, *308*(5725), 1127–1133, doi:10.1126/science.1112250.

Lüschen, E., C. Mueller, H. Kopp, M. Engels, R. Lutz, L. Planert, A. Shulgin, and Y. Djajadihardja (2010), Structure, evolution and tectonic activity at the eastern Sunda forearc, Indonesia, from marine seismic investigations, *Tectonophysics*, doi:10.1016/j.tecto.2010.06.008, in press.

Lynnes, C. S., and T. Lay (1988), Source process of the great 1977 Sumba earthquake, *J. Geophys. Res.*, *93*(B11), 13,407–13,420, doi:10.1029/JB093iB11p13407.

Moore, G. F., N. L. Bangs, A. Taira, S. Kuramoto, E. Pangborn, and H. J. Tobin (2007), Three-dimensional splay fault geometry and implications for tsunami generation, *Science*, *318*, 1128–1131, doi:10.1126/science.1147195.

Mueller, C., and S. Neben (Eds.) (2006), *Cruise report: SO190 Leg 1: Seismic and geoacoustic investigations along the Sunda-Banda Arc transition*, 142 pp., Bundesanstalt für Geowiss. und Rohstoffe, Hannover, Germany.

Müller, C., et al. (2008), From subduction to collision: The Sunda-Banda arc transition, *Eos Trans. AGU*, *89*(6), 49–60, doi:10.1029/2008EO060001.

Newcomb, K. R., and W. R. McCann (1987), Seismic history and seismotectonics of the Sunda arc, *J. Geophys. Res.*, *92*, 421–439, doi:10.1029/JB092iB01p00421.

Oleskevich, D. A., R. D. Hyndman, and K. Wang (1999), The updip and downdip limits to great subduction earthquakes: Thermal and structural models of Cascadia, south Alaska, SW Japan, and Chile, *J. Geophys. Res.*, *104*(B7), 14,965–14,991, doi:10.1029/1999JB900060.

Parker, R. L. (1973), The rapid calculation of potential anomalies, *Geophys. J. R. Astron. Soc.*, *31*, 447–455, doi:10.1111/j.1365-246X.1973.tb06513.x.

Peacock, S. M. (2001), Are the lower planes of double seismic zones caused by serpentine dehydration in subducting oceanic mantle, *Geology*, *29*(4), 299–302, doi:10.1130/0091-7613(2001)029<0299:ATLPOD>2.0.CO;2.

Ranero, C. R., J. Phipps-Morgan, K. McIntosh, and C. Reichert (2003), Bending-related faulting and serpentinzation at the Middle America trench, *Nature*, *425*, 367–373, doi:10.1038/nature01961.

Ranero, C. R., I. Grevemeyer, H. Sahling, U. Barckhausen, C. Hensen, K. Wallmann, W. Weinrebe, P. Vannucchi, R. von Huene, and K. McIntosh (2008), Hydrogeological system of erosional convergent margins and its influence on tectonics and interplate seismogenesis, *Geochem. Geophys. Geosyst.*, *9*, Q03S04, doi:10.1029/2007GC001679.

Rutherford, E., K. Burke, and J. Lytwyn (2001), Tectonic history of Sumba Island, Indonesia, since the Late Cretaceous and its rapid escape into forearc in the Miocene, *J. Asian Earth Sci.*, *19*, 453–479, doi:10.1016/S1367-9120(00)00032-8.

Rüpke, L. H., J. P. Morgan, M. Hort, and J. A. D. Conolly (2004), Serpentine and the subduction zone water cycle, *Earth Planet. Sci. Lett.*, *223*, 17–34, doi:10.1016/j.epsl.2004.04.018.

Schlüter, H. U., C. Gaedicke, H. A. Roeser, B. Schreckenberger, H. Meyer, C. Reichert, Y. Djajadihardja, and A. Prexl (2002), Tectonic features of the southern Sumatra-western Java forearc of Indonesia, *Tectonics*, *21*(5), 1047, doi:10.1029/2001TC901048.

Shulgin, A., H. Kopp, C. Mueller, E. Lüschen, L. Planert, M. Engels, E. R. Flueh, A. Krabbenhoeft, and Y. Djajadihardja (2009), Sunda-Banda arc transition: Incipient continent-island arc collision (northwest Australia), *Geophys. Res. Lett.*, *36*, L10304, doi:10.1029/2009GL037533.

Sibuet, J.-C., et al. (2007), 26th December 2004 great Sumatra–Andaman earthquake: Co-seismic and postseismic motions in northern Sumatra, *Earth Planet. Sci. Lett.*, *263*, 88–103, doi:10.1016/j.epsl.2007.09.005.

Simons, W. J. F., et al. (2007), A decade of GPS in Southeast Asia: Resolving Sundaland motion and boundaries, *J. Geophys. Res.*, *112*, B06420, doi:10.1029/2005JB003868.

Smyth, H. R., P. J. Hamilton, R. Hall, and P. D. Kinny (2007), The deep crust beneath island arcs: Inherited zircons reveal a Gondwana continental fragment beneath East Java, Indonesia, *Earth Planet. Sci. Lett.*, *258*, 269–282, doi:10.1016/j.epsl.2007.03.044.

Smyth, H. R., R. Hall, and G. J. Nichols (2008), Cenozoic volcanic arc history of East Java, Indonesia: The stratigraphic record of eruptions on an active continental margin, in *Lessons From the Stratigraphic Record in Arc Collision Zones*, edited by A. E. Draut, P. D. Clift, and D. W. Scholl, *Spec. Pap. Geol. Soc. Am.*, 436, 27–54, doi:10.1130/2008.2436(10).

Spence, W. (1986), The 1977 Sumba earthquake series: Evidence for slab pull force acting at a subduction zone, *J. Geophys. Res.*, *91*(B7), 7225–7239, doi:10.1029/JB091iB07p07225.

Špičák, A., V. Hanuš, and J. Vaněk (2007), Earthquake occurrence along the Java trench in front of the onset of the Wadati-Benioff zone: Beginning of a new subduction cycle?, *Tectonics*, *26*, TC1005, doi:10.1029/2005TC001867.

Tatsumi, Y., H. Shukuno, K. Tani, N. Takahashi, S. Kodaira, and T. Kogiso (2008), Structure and growth of the Izu-Bonin-Mariana arc crust: 2. Role of crust-mantle transformation and the transparent Moho in arc crust evolution, *J. Geophys. Res.*, *113*, B02203, doi:10.1029/2007JB005121.

Toomey, D. R., and G. R. Foulger (1989), Tomographic inversion of local earthquake data from the Hengill-Grensdalur central volcano complex, Iceland, *J. Geophys. Res.*, *94*, 17,497–17,510, doi:10.1029/JB094iB12p17497.

Van der Werff, W. (1995), Structure and morphotectonics of the accretionary prism along the eastern Sunda–western Banda Arc, *J. Southeast Asian Earth Sci.*, *11*, 309–322, doi:10.1016/0743-9547(94)00038-G.

Wiener, N. (1949), *Extrapolation, Interpolation, and Smoothing of Stationary Time Series*, John Wiley, New York.

E. R. Flueh, H. Kopp, A. Krabbenhoeft, L. Planert, and A. Shulgin, IFM-GEOMAR, Leibniz Institute of Marine Sciences at the University of Kiel, Wischhofstr. 1-3, D-24148, Germany. (lplanert@ifm-geomar.de)

E. Lueschen and C. Mueller, BGR, Federal Institute for Geosciences and Natural Resources, Stilleweg 2, D-30655 Hannover, Germany.

Y. Djajadihardja, BPPT, Agency for the Assessment and Application of Technology, Jl. M.H. Thamrin No. 8, Jakarta 10340, Indonesia.